Contributions of downstream baroclinic development to strong southern hemisphere cut-off lows

Article

Accepted Version

Quarterly Journal of the Royal Meteorological Society
A journal of the atmospheric sciences and physical oceanography
RMetS

Contributions of downstream baroclinic development to strong Southern Hemisphere Cut-off Lows

Journal:	*QJRMS*
Manuscript ID	QJ-20-0314.R5
Wiley - Manuscript type:	Research Article
Date Submitted by the Author:	13-Oct-2021
Complete List of Authors:	Pinheiro, Henri; National Institute for Space Research, Center for Weather Forecast and Climatic Studies (CPTEC) Hodges, Kevin; The University of Reading, Dept. of Meterology Gan, Manoel; National Institute for Space Research, Center for Weather Forecast and Climatic Studies (CPTEC) Ferreira, Sergio; National Institute for Space Research, Center for Weather Forecast and Climatic Studies (CPTEC) Andrade, Kelen; National Center for Monitoring and Early Warning of Natural Disaster
Keywords:	Cut-off Lows, Energetics, Eddy Kinetic Energy, Ageostrophic Flux Convergence, Baroclinic Conversion, Downstream Development
Country Keywords:	AAA - No country

Contributions of downstream baroclinic development to strong Southern Hemisphere Cut-off Lows

Henri Rossi Pinheiro[1], Manoel Alonso Gan[1], Kevin Ivan Hodges[2], Sergio Henrique Soares Ferreira[1], and Kelen Martins Andrade[3]

[1]Center for Weather Forecast and Climate Studies (CPTEC), National Institute for Space Research (INPE), Sao Jose dos Campos, SP, Brazil

[2]Department of Meteorology, The University of Reading, Reading, United Kingdom

[3]National Center for Monitoring and Early Warning of Natural Disaster (CEMADEN), Sao Jose dos Campos, Brazil

Corresponding author: henrirpinheiro@gmail.com

Telephone Number: +55 12 3208-6000

ORCID: 0000-0003-4363-3206

Abstract

Cut-off Lows (COLs) in the Southern Hemisphere and the mechanisms involved in their development are investigated in detail using the eddy kinetic energy (EKE) budget applied to data from the ERA-Interim reanalysis. This approach considers the most important processes that are typical for the evolution of midlatitude disturbances such as the baroclinic (BRC) and barotropic (BRT) conversions, and the ageostrophic flux convergence (AFC), known as downstream development. Composites of the volume-integrated EKE and its components are evaluated based on the 200 most intense SH COLs (> 98th percentile) observed in a 36-yr period. Results show that the AFC together with the BRC conversion are the most important contributor to the EKE growth for the COLs, characterizing the downstream baroclinic development. The AFC plays an important role in genesis and intensification phases of the COLs, while the BRC conversion is important for the system maintenance. The dissipation of the COLs occurs due to dispersive fluxes (ageostrophic flux divergence) together with other processes not directly computed in the EKE equation, such as friction and latent heat release which are problematic in reanalysis datasets. The BRT conversion contributes negatively to the COL development by transferring EKE to the zonal flow kinetic energy, though this is not enough to dampen the intensification. Regional differences were found in the energetics, indicating that COLs originating upstream of the continents are clearly dominated by ageostrophic fluxes, while the systems over the Australian region are mostly driven by baroclinic processes.

Keywords: Cut-off Lows; Energetics, Eddy Kinetic Energy, Baroclinic Conversion, Ageostrophic Flux Convergence.

1 Introduction

Over the past several decades, Cut-off Low (COL) systems have been attracting increasing attention from the forecasting and research communities, mainly because of the severe impacts that intense storms of this type can have on human activities. In the Southern Hemisphere (SH), COLs are one of the major synoptic-scale systems that contribute to the rainfall in subtropical regions (Llasat et al. 2007; Singleton and Reason 2007; McInnes and Hubbert 2001). COLs have been found to be responsible for over half of the total precipitation in southeastern Australia (Pook et al. 2006), standing out as being the main controlling factor for the interannual variability of rainfall (Risbey et al. 2009). Moreover, COLs are distinct systems that can cause unusual precipitation in arid regions such as in the Namib and Kalahari Deserts in southern Africa (Muller et al. 2008) and the Atacama Desert in the north Chilean Andes (Bozkurt et al. 2016).

During the past two or three decades, a variety of observational and modelling studies have been undertaken to guide our knowledge of COLs. Great efforts have been made to better understand COLs in regard to their typical behavior and the different physical and dynamical processes associated with them. A typical COL differs from the cold-core vortices found at higher latitudes as COLs generally originate equatorward of the main westerlies. The main climatological features of COLs such as where they are usually found, their trajectories, life span and seasonal variability are generally accepted in the published literature (Fuenzalida et al. 2005; Nieto et al. 2008; Reboita et al. 2010; Pinheiro et al. 2017), but the processes that control the intensification and maintenance of COLs have not previously been investigated extensively. A better understanding of the mechanisms that typically control the development of COLs may help to improve their representation in models and enable improved forecasting of COLs.

A large body of literature has documented the evolution of mid-latitude disturbances since the classical studies of Charney (1947), Eady (1949) and Kuo (1949), contributing to our understanding of baroclinic growth and barotropic decay. Later, other factors have been considered that may influence the development of cyclonic disturbances in subtropical and mid-latitudes, such as diabatic processes (Davis et al. 1993; Martínez-Alvarado et al. 2014), surface fluxes (Kuo et al. 1991; Nogués-Paegle and Mo 1997; Dal Piva et al. 2011), topography (Buzzi et al. 1987; Hayes et al. 1987; Gan and Rao 1994; Mikyfunatsu et al. 2004), and the interaction between upper-tropospheric potential vorticity (PV) with lower-tropospheric cyclonic features (Hoskins et al. 1985; Mikyfunatsu et al. 2004).

Although numerous previous studies have demonstrated that the contribution of baroclinic processes are the most important for the growth of mid-latitude disturbances, the concept based on the idea of atmospheric energy dispersion (Rossby 1945; Yeh 1949), the so-called downstream development (Simmons and Hoskins 1979), has emerged as an essential mechanism for the development and maintenance of synoptic-scale systems. According to this theory, the development of baroclinic eddies is the result of the energy dispersed from decaying systems upstream, which propagate eastward with a nearly Rossby wave group velocity (Pedlosky 1987; Chang and Orlanski 1994). Orlanski and Sheldon (1995) observed that cyclone waves grow initially due to the upstream energy source and later because of the baroclinic conversion (EKE growing with ascent in the warm air and descent in the cold air) referred to as downstream baroclinic development. Motivated by this context, other authors have made use of the concept of downstream energy dispersion to provide a dynamical interpretation of the baroclinic disturbances based on observations (Chang 1993; 2000; Danielson et al. 2004; 2006; Decker and Martin 2005; Dal Piva et al. 2010;

Rivière et al. 2015) or model simulations (Hoskins and Simmons 1979; Orlanski and Chang 1993; Papritz and Schemm 2013; Schemm et al. 2013).

The perspectives obtained from the concept of downstream baroclinic development have motivated the use of the local eddy kinetic energy (EKE) equation described by Orlanski and Katzfey (1991) to explore the energy budget of cyclones, although very few attempts have been made to investigate the energetics of COLs. Nevertheless, there are a few studies, for example the study of Gan and Dal Piva (2013) who used the National Centers for Environmental Prediction (NCEP) Department of Energy (DOE) reanalysis to analyse the evolution of a COL in the South Pacific Ocean. They found some differences in terms of the dominant mechanisms active in the COL studied compared to typical extratropical cyclones, as the ageostrophic flux convergence (AFC) was the main mechanism responsible for the EKE growth of the COL, whereas the baroclinic (BRC) conversion played a secondary role, and was only important for the genesis. The barotropic (BRT) term remained negative during the whole life cycle, representing an important dissipative mechanism. These results were confirmed in a composite study using fifty cases of COLs that occurred in the South Pacific Ocean (Gan and Dal Piva 2016).

In a similar study, but using the Lorenz energetics (Lorenz 1955), Pinto and da Rocha (2011) found that a particular disturbance associated with a mid-level COL located off the southern Brazilian coast intensified due to the strong influx of available potential and kinetic energy into the domain. These findings are consistent with the recent demonstration that the zonal flow influences the COL development by advecting zonal momentum from the large-scale jet streak in a nearly eastward direction (Ndarana et al. 2020). In addition, earlier studies have demonstrated that the downstream amplification mechanism associated with upper-level cold lows off Northeast Brazil is a result of

Rossby, and mixed Rossby-gravity wave dispersion (Silva Dias et al. 1983) with a dominant period of 3-6 days with peak activity during the summer (Magaña and Yanai 1995; Yanai and Maruyama 1966). This type of disturbance can act as a precursor to upper tropospheric vortices triggered by various processes such as lateral forcing (Mak 1969), thermal forcing (Lamb 1973), and wave-CISK (conditional instability of the second kind) (Hayashi 1970).

While the studies of Gan and Dal Piva (2013; 2016) have demonstrated that COL development is indeed dominated by the energy originating from upstream regions rather than directly from baroclinic processes, it is not clear whether the results therein are robust enough to represent the energetics over a larger number of COLs, including those located in other regions in the SH, because of the different nature of COLs, as recently discussed by Pinheiro et al. (2020b). Given the poor understanding of the energetics of COLs due to the limited sample size used in previous studies, the most relevant scientific questions addressed in this paper are:

1. What are the main development mechanisms of the most intense SH COLs?
2. Which mechanisms are the most important at specific stages of the COL life cycle, and how do these mechanisms interact dynamically with each other?
3. How do the mechanisms of COL development vary regionally?

The focus of the study is on the strongest systems because COLs generally cause significant precipitation only if they are strong enough to be connected to cyclonic features at lower levels (Pinheiro et al. 2020b), and which may lead to significant moisture and heat transport from tropical latitudes into the system.

The paper continues in Section 2 with a description of the reanalysis dataset and the methodologies used to identify and track COLs and to compute the EKE budget.

Section 3 presents the analysis of the composite energetics of austral COLs through horizontal (vertically integrated quantities) and vertical cross-section fields. Section 4 gives a summary of the main results and conclusions, and recommendation for future work.

2 Data and Methodology

2.1 Description of the ERA-Interim reanalysis

The study uses six-hourly gridded data from the European Centre for Medium-Range (ECMWF) Interim (ERA-Interim) reanalysis to identify and track SH COLs and to compute energy budgets (from 1000 hPa to 100 hPa) during a 36-yr period (1979-2014). Following Pinheiro et al. (2020b, and references therein), we have chosen 300 hPa relative vorticity and geopotential to analyze COLs as they are more frequent and intense at this level. The ERA-Interim reanalysis for the satellite era (1979 onward) uses a spectral model with TL255 horizontal resolution (~80 km) and 60 vertical hybrid levels with model top at 0.1 hPa. ERA-Interim is produced with four-dimensional variational data assimilation (4D-Var) system to assimilate the disparate quality controlled observations. A description of the ERA-Interim reanalysis is given by Dee et al. (2011). This dataset was chosen because this is in good agreement with other contemporary reanalyses regarding the identification of COLs (Pinheiro et al. 2020a).

2.2 Track and identification

In this study, the tracking algorithm described by Hodges (1995; 1999) is applied to the ERA-Interim reanalysis relative vorticity and geopotential data at 300hPa to track and identify SH COLs using the tracking criteria presented in Pinheiro et al. (2019) and the detection criteria based on the horizontal winds around the vortex center to separate COLs from other cyclonic systems. Before the tracking, the vorticity field is spectrally

truncated to T42 for vorticity as vorticity is a noisy field, while the geopotential field is spectrally truncated at T63 as this is a smoother field. The tracking is performed on the two fields independently using six-hourly data for the 300-hPa relative vorticity (ξ_{300}) and 300-hPa filtered geopotential (Z'_{300}). Filtered geopotential is obtained by removing the zonal mean from the geopotential data for each time step and for each latitude, in order to facilitate identification. The initial identification and tracking are as reported in Pinheiro et al (2019). To ensure that the ξ_{300} and Z'_{300} minima are cut-off from the westerlies, restrictive conditions are imposed to the horizontal wind components (u, v) in four offset points located 5º geodesic from the COL center which are 0° (u > 0), 90° (v < 0), 180° (u < 0), and 270° (v > 0) relative to North. Finally, we discard short tracks (those with lifetimes less than 1 day) to avoid noise in the composites.

2.3 Composite energetics

The energetics of extreme SH COLs are examined using composites of the 200 most intense systems that are identified in both ξ_{300} and Z'_{300}, which exceed the 98th percentile of the total number of matched COLs in the SH. Common systems are identified using the same matching method as used in Pinheiro et al. (2020b). An overview of the trajectories used in the composites is given in Fig. 1. The analysis is based on the eddy kinetic energy (EKE) equation developed by Orlanski and Katzfey (1991) and modified by Chang (2000). This is done by partitioning the processes associated with the COL development into mean flow and perturbations (eddies), and then analyzing individually the components of the EKE, which are represented in Equation 1 as follows:

$$\frac{\partial\langle K'\rangle}{\partial t} = -\langle\nabla.\vec{V}K'\rangle - \left\langle\nabla.\overrightarrow{V'_a\phi'}\right\rangle - \langle\omega'\alpha'\rangle - \left\langle\overrightarrow{V'}.\left(\vec{V}'_3.\nabla_3\right)\vec{\overline{V}} + \overrightarrow{V'}.\overrightarrow{\left(\overrightarrow{V'_3}.\nabla_3\right)V'}\right\rangle - [\omega K']\big|_B + [\omega K']\big|_T - [\omega'\phi']\big|_B + [\omega'\phi']\big|_T + \langle\nabla.\vec{V}_V K'\rangle + \left[\left(\frac{\partial p_s}{\partial t} + \vec{V}_V.\nabla p_s\right)K'\right]\Big|_B + \langle RES\rangle \quad (1)$$

In Equation 1, K represents the kinetic energy, α the specific volume, $\vec{V}$ the horizontal wind, ϕ the geopotential, ω the vertical velocity, and p_s the surface pressure. The overbar denotes the time-mean flow calculated for each month averaged over 28-31 days for the 6-hourly data. This is done separately for each individual month and year. The primes represent the terms associated with the eddies (referring to the deviation from the mean state), the superscript 3 the three-dimensional vector, the subscript a the ageostrophic component, and the subscript v volume displacement velocity. The symbols ⟨⟩ and [] represent volume integrals taken from the bottom (chosen to be the surface pressure, subscript B) to the top (chosen to be the 100 hPa level, subscript T).

The term on the left-hand side of Equation 1 is the local tendency of EKE. The first term on the right-hand side is the EKE flux convergence (KFC) which is associated with the advective fluxes (Chang 2000). The 2nd term is the ageostrophic flux convergence (AFC) due to the transfer of energy through the wave dispersion, known as downstream development (Orlanski and Sheldon 1993). The 3rd term is the baroclinic (BRC) conversion that is associated with the thermally-direct circulation with warm air rising and cold air sinking. The 4th and 5th terms are the Reynolds stress or barotropic (BRT) conversion which are associated with the horizontal wind shear. The BRT process represents the rate of conversion from zonal to eddy kinetic energy associated with transports of momentum. In mid-latitude transient disturbances the BRT conversion is often related to system dissipation, though it may contribute to intensify the disturbance in some tropical disturbance such as tropopause vortices near the North-eastern Brazil region (Mishra et al. 2001). The 6th and 7th terms are the vertical advection of energy through the lower boundary (i.e., surface pressure) and the upper boundary (i.e., 100 hPa). The 8th and 9th terms represent the energy inflow through the bottom and top boundaries due to the ageostrophic fluxes. The 10th term is the energy

flux due to movement of the volume integration, whereas the 11th and 12th terms represent the energy variation due to the change in mass inside the volume integration. The 10th-12th terms are not computed in this study due to the complexity in estimating the energy fluxes associated with the movement of volume integrals. The 13th term is the budget residual (RES) representing the mechanisms not explained in Equation 1 such as friction, errors in the calculation of diabatic terms in reanalysis, sub-grid flows and errors introduced by numerical methods, such as interpolation and finite differences. Another contributor to the residual may be associated with the analysis increment in the reanalysis data which results from data assimilation procedures, which may affect the energetics.

The tendency of EKE can be calculated using two different methods: the first one uses a centered-time difference between the previous and subsequent time steps to compute the left-hand side (LHS, observed tendency) of Equation 1, resulting in 12-h differences in EKE. This is performed by considering the EKE in the volume that moves following the system. The second way is to compute the tendency by summing all the terms on the right-hand side (RHS, computed tendency) of Equation 1, except the 10th-12th terms which will be part of the RES. The RES is estimated by the difference between the two methods described above, i.e., the LHS minus the RHS.

The energetics are examined using a compositing methodology that has been previously applied to tropical and extratropical cyclones (Bengtsson et al. 2007; Catto et al. 2010) and more recently to subtropical COLs (Pinheiro et al. 2020b). For the budget calculations this is done by referencing the components of the EKE budget to a radial grid with a prescribed radius centered on the COL center. Composites are also produced for specific times relative to the time of maximum intensity of the COLs with respect to ξ_{300}. For the spatial composites, it is more convenient to use a rectangular grid, not

rotated according to the system propagation direction as in Catto et al (2010), which allows the examination of the COL horizontal tilt throughout the life cycle.

Energetic composites are vertically integrated from 1000 hPa (or surface) to 100 hPa, where the surface depends on the topography obtained from the reanalysis. This is particularly important over the mountain areas such as the Andes Cordillera, so that the energy is only computed above the surface. For more specific analyses, the energetics are also computed for each pressure level separately in exactly the same way as done by Chang (2000) applying his Equation 1, which is similar to our Equation 1 but without the 10th, 11th and 12th terms. This allows us to examine how each term of the EKE equation behaves in a vertical cross-section.

The area of the cylinder used for the calculations is considered to be fixed at a suitable prescribed radius, which will is chosen according to the practical purpose of the research and after considering how the residual in the EKE budget is affected by the chosen radial distance. Perhaps the main difference in approach between this study and previous ones is that we use a fully objective method to identify and track the system of interest, so that the energetics are computed directly over the COL center, avoiding subjective decisions on the system location, and minimizing contributions from advection of EKE through the boundaries. Moreover, the use of the algorithm facilitates using a larger number of systems for the compositing in comparison to manual procedures used to create composites, e.g., in Danielson et al. (2004) and Gan and Dal Piva (2016). For a regional analysis, the main genesis areas are identified and the tracks that have their genesis over a spherical region (radius=10^{o}) centered on the maxima genesis are selected. This is done considering all identified COLs rather than using the strongest ones to ensure the analyses represent the typical EKE budget in each region.

3 Results

3.1 Frequency distribution

Given that the energetics may vary widely over all the SH COLs, we will first present an overview of the frequency distributions of the main energetic terms for all the SH COLs (total number is 11,542 tracks) identified in both ξ_{300} and Z'_{300}, i.e are identical systems in both fields, across the period 1979-2014. After a brief look at all the computed terms of Equation 1, we analyze the dominant terms through the distribution of the along-track mean values for the BRC, BRT and AFC terms (Fig. 2), which are integrated from the surface to 100 hPa and averaged over a 15° spherical cap region centered on each COL center. A visual inspection of the energetics revealed that the radial distance of 15° is appropriate to capture the main energy centers that control the COL development. The frequency distributions indicate that most storms have positive values of the BRC and AFC terms, while the BRT term is dominated by negative values, though variations in the distributions of these terms are observed. It is therefore apparent that SH COLs mainly intensify through the BRC and AFC mechanisms, although the contribution of these terms varies through time, as will be shown in the next section.

3.2 The residual problem

Before examining each term of the EKE budget, we provide a discussion of the residual which represents a factor of uncertainty in our work, existing mainly because of energy forcings that are not included in Equation 1 such as the friction and errors in estimating the diabatic processes by reanalysis (including the radiative, latent and sensible heat fluxes), but also because of energy fluxes related to the volume integration displacement and the variation of the mass in the volume, which are represented by the 10-12th terms. Inconsistencies can also be a result of the numerical error in the finite difference equations and the analysis increment in the reanalysis data. The residual is first assessed

to determine its magnitude for the strongest SH COLs using different radial distances from the vortex center, such as 5º, 10º, 15º, 20º and 25º in geodesic distances (Fig. 3a). This is done to provide an overview of the possible implications of the choice of boundaries for the residual.

Fig. 3a shows that the estimation of the residual in the COLs depends on the size of the measurement volume in which the values are calculated. In general, the larger the horizontal area the smaller the amplitude of the residual throughout the COL lifecycle. The largest amplitude of the residual is observed using 5º and 10º, but it decreases with increasing area. The fact that the residual amplitude reduces with increasing volume may be related to the transfer of energy across the boundaries (Muench 1965; Michaelides 1987) where part of this transfer is represented by the energy flux (AFC and KFC terms). Thus, the energy transport through the borders is probably more important for relatively small regions (e.g., 5º or 10º geodesic radius) than in the outer regions where the energy fluxes are relatively weak. However, if we set a large value for the area, mechanisms that operate outside the system (i.e., other systems may be included) may affect the EKE budget when using a large domain to perform the volume integration.

It can be seen from Fig. 3a that the residual is negative (rhs larger than lhs) throughout the life cycle with radii equal or greater than 20 degrees and negative for most of the life cycle with radii smaller than 20 degrees. The largest residuals are found in the decay stage of the lifecycle. One reason for this “energetic imbalance” may be the unknown contribution of the frictional dissipation, which represents an important energy sink for the disturbance, though these effects are suggested to be not significant near the tropopause (Cavallo and Hakim 2010). In a brief period of the COL development (from ‘day -2’ to ‘zero’) the residual remains positive for the small radii (e.g., 5º, 10º, 15º),

which means there are other mechanisms that act as energy sources but that are not directly computed or they are not correctly reproduced by the reanalysis, such as the radiative cooling near the vortex, which was found to be important to intensify tropopause polar vortices (Cavallo and Hakim 2010). This will be discussed later with regard to the spatial pattern of the residual. Despite the large variation in amplitude, the average residual computed over the whole life cycle is not sensitive to the radius, as shown in the legend of Fig. 3a.

The EKE tendency is calculated using two different methods (LHS and RHS of Equation 1), as described in the methodology. These are shown in Fig. 3b, where a significant correspondence for the EKE tendency between the RHS and LHS terms is found during the growth phase of the COLs (defined as the time before the maximum intensity of each COL), but marked differences occur in the decay phase (defined as the time after the maximum intensity of each COL) that results in the large residual. The difference between the LHS and RHS is negative when the COLs are decaying, and this is probably related to effects associated with the friction and errors in diabatic heating near the COL center. This energetic inconsistency is clearly evident in the curve of EKE tendency obtained with the RHS when positive values appear during the decay phase, indicating that there may exist dissipative mechanisms that are not included in the formulation. The temporal evolution of the total EKE in the COLs (Fig. 3b) indicates that the peak EKE coincides in time with the maximum intensity of the ξ_{300} COLs, which is consistent with our expectation.

The residual is now investigated by examining its time evolution in terms of the spatial distribution for the period of two days (48 hours) before and after the peak intensity. The distribution of the residual term is presented with the corresponding standard deviation (Fig. 4) to examine the spread (dispersion) within the sample. This shows that

the negative residual maximizes immediately downstream of the COLs, particularly in the mature and decay stages, and this suggests the presence of dissipation mechanisms that are not considered in our approach or they are not well represented in the reanalysis. The large negative residual seems to be related to issues in the estimation of latent heating release by the reanalysis, which we can also infer to be a fundamental diabatic forcing in COLs. Particularly east of the COL, latent heat release may contribute to the generation of eddy available potential energy (EAPE) and later converted to EKE by baroclinic conversion where warm ascent air is diagnosed (cf. Fig. 7b and Fig. 8b, which the ascent and precipitation is presumably collocated with warm air; see also a discussion of the precipitation in Pinheiro et al. (2020b)). This assumption is intuitive considering that the precipitation in COLs (see Fig. 5 of Pinheiro et al. 2020b) spatially and temporally coincides with the spatial pattern of the negative residual energy. While diabatic heating does not directly contribute to the EKE budget due to the fact that the EKE budget does not involve any diabatic heating terms, errors in the reanalyses due to miss-representation of diabatic heating can easily introduce uncertainties in the energetic framework, because diabatic heating can generate EAPE and then be converted to EKE by means of baroclinic conversion (Orlanski and Katzfey 1991). This is discussed further below.

Positive residual is found mainly upstream of the vortex center during the growth stage, which seems to be placed in the region where the EAPE is converted to EKE in COLs (Ndarana et al. 2021). We hypothesize that the likely source of positive residual may be related to issues in estimating the radiative cooling rates in the reanalysis, which becomes less important as the cold core warms up. The results described above support the idea that the latent heating acts to weaken the upper-level cold-core vortex (Garreaud and Fuenzalida 2007; Sakamoto and Takahashi 2005; Cavallo and Hakim

2010), while radiative cooling is important for the system intensification (Cavallo and Hakim 2010).

The fact that the EKE budget does not contain any diabatic heating terms implies that there should be no direct influence of diabatic processes on the EKE budget. But this would only be true on the assumption that the data used to compute the EKE budget is all self-consistent such as would come from a free running model. However, this is not the case with a reanalysis where a model first guess is adjusted towards the observations, which vary in space and time, so that the analysis increment is strongly dependent on the inhomogeneous observations, some of which are related to diabatic processes (e.g., humidity). It has been shown in other studies (Guo and Chang, 2008; Privé and Errico 2013; https://confluence.ecmwf.int/display/FUG/4.2+Analysis+Increments) that the increment can be large around regions of strong convection where the model depends on parameterized diabatic processes and in addition the European Centre for Medium-Range Weather Forecasts (ECMWF) model is a hydrostatic model which means that miss-representation of these processes can result in large differences between the model first guess and observations resulting in a large analysis increment. Differences can also occur due to how certain observations (e.g., satellite data) are obtained and how they are assimilated. This is likely to vary from time step to time step in the analysis as the observations vary introducing noise into the reanalysis data which could be large if the increments are large. This will affect all the data used in the budget calculation, including the finite difference on the LHS, resulting in a contribution to the budget residual. In addition, the analysis increments will likely vary through the COL lifecycle as the influence of diabatic processes become important which is why we hypothesize that the residual is large in the region of strong precipitation. These findings reinforce

the importance of diabatic processes for the development of COLs. The relative contribution of diabatic cooling and heating could be quantified using a numerical model, but this is beyond the scope of this study and is a matter for further investigation.

3.3 Energetics for strong Cut-off Lows

The relative contributions of the main mechanisms for the development of the strongest SH COLs are analyzed in this section in terms of the EKE budget. Given the set of COLs is the same as used in Pinheiro et al. (2020b), their findings will be considered as the basis to serve as information for the discussion presented in this paper. It can be seen from Fig. 5 that the AFC is by far the most important contributor to the EKE growth. The transport of energy due to ageostrophic fluxes occurs with the group velocity of Rossby waves and represents the radiative part of the total energy flux that exists due to the dispersive nature of the atmospheric waves (Pedlosky 1987; Chang 2000). The AFC acts to import EKE from upstream systems in the early stages of the COL lifecycle, while strong dispersive EKE fluxes occur in the decay phase, serving as the primary mechanism responsible for the increase/decrease of energy for the COL. The AFC decreases in the system region as the COL approaches its maximum intensity. At this time, the BRC conversion becomes the most important mechanism to maintain the COL, converting eddy available potential energy (EAPE) to EKE (Oort and Peixoto 1983). The EAPE is also generated by diabatic heating, particularly during the mature and decay stages of a COL, which is the time of the peak precipitation. The major source of diabatic heating is generally found in the warm sector of midlatitude cyclones (Carlson 1991). This is similar to what happens in the most intense COLs, where most precipitation occurs on the east side, and this may contribute to enhance the horizontal temperature gradient. However, when the convection occurs near the COL center, the

diabatic heating tends to warm the cold core leading to vortex dissipation (Kousky and Gan 1981). The composite of the BRC term shows two peaks separated in time by approximately four days. This behavior is likely to be caused by diabatic forcing and will be discussed later in the paper.

The other part of the total energy flux is the advective flux (KFC) that has a large magnitude, but only contributes to displace the EKE center (Chang 2000). This is attributed to the movement of energy centers rather than the intensification of the system, where its movement is given by the phase velocity (Chang and Orlanski 1993). Positive values of KFC are seen during the growth stage and imply that the energy is being advected into the COL, while negative values means that the energy is advected out of the system during the decay stage. The BRT term remains negative during the whole development phase, representing the main energy sink. Note that the BRT conversion acts in opposition to the EKE growth, but this is not enough to prevent the intensification of the COLs. In the decay, the BRT is nearly zero, thereby the AFC and other dissipative mechanisms such as friction and diabatic heating are most important in dissipating the COLs. The regional analysis undertaken later in this paper will demonstrate that the damping mechanisms will be greater the greater the intensity of the ageostrophic flow.

The results partly confirm earlier findings (Gan and Dal Piva 2013; 2016) concerning the dominance of the ageostrophic flux convergence (divergence) to the growth (decay) of the COLs. However, our results reveal that the BRC conversion plays a greater contribution to the development of COLs, particularly to their maintenance. The sum of the energy gain over the entire life cycle of the COLs corresponds to 58.3 x 10^{15} Joule for the AFC and 51.8 x 10^{15} Joule for the BRC term. Despite the smaller amplitude of the BRC term compared to the AFC term (see Fig. 5), the former is the only term of the

EKE budget that remains positive during the whole life cycle, characterizing the main EKE source for the COLs and the main mechanism for their maintenance.

Recent studies have demonstrated the role of the jet stream on the development of COLs in particular locations in the SH (Gan and Dal Piva 2013; 2016; Ndarana et al. 2020; 2021). We now compare the results from the previous papers against our findings for the strongest systems and discuss how the jet stream affects the COL development in terms of the EKE perspective. These features are shown in Fig. 6 as the temporal evolution of spatial composites. The initial stage of the COL lifecycle ($T = -48h$) begins with a pre-existing upper-level trough associated with a fairly broad EKE center on the west side and a weaker EKE center on the east side of the trough. In the following discussion we will also use the terms "rear" and "front" interchangeably in referring to "west" and "east", respectively. The wind speed field exhibits a split jet structure caused by the convergence of vorticity advection (Ndarana et al. 2020). The split jet formation deepens the trough-ridge system, promoting an influx of EKE from the midlatitude jet into the rear side of the COL. The rear energy center grows vigorously over the next day ($T = -24h$) by receiving EKE from the upstream midlatitude center by means of ageostrophic fluxes. As the rear EKE center matures, it loses energy downstream to intensify the front EKE center. The rear EKE center starts decaying just before the maximum intensity in the ξ_{300}, when there is no longer a supply of energy from the upstream midlatitude system and also as a consequence of its own export of energy downstream. At the mature stage ($T = 0$), the east EKE center reaches its maximum intensity and then starts to decay. The decaying stage ($T \geq 24h$) is marked by an overturning flux as the EKE centers on the east and west sides merge with each other to form a single center in the southern sector of the COL, resembling the case in Gan and Dal Piva (2013) their Fig. 4. Similarly to Ndarana et al. (2020;

2021), the midlatitude jet propagates in the south-eastward direction during the early stage and then exhibits a more zonal orientation in the late stage. The propagation of the jet streak favors anticyclonic wave breaking, indicated by a deformation of isentropic PV contours (blue contour), leading to the advection of the stratospheric PV anomaly into the subtropical troposphere.

The composite evolution of the strongest SH COLs is now examined separately for the three main terms of the EKE budget (AFC, BRC and BRT) using vertically averaged fields (Fig. 7) and vertical cross-sections in the W-E direction (Fig. 8). The horizontal and vertical cross-sections are conveniently discussed together. The vertical cross-sections were examined along a line west-east at latitude zero (i.e., where the vorticity center is located in each COL) as well as considering averages over latitudinal bands of different widths. We found that the gradient of the EKE is significantly enhanced near the COL center, thus the vertical cross-sections provided here are taken through a line west-east at latitude zero. Fig. 7 shows that the evolution of the strong COLs is preceded by an upstream baroclinic wave, following the idealized model described by Orlanski and Sheldon (1995). The source region along the midlatitude jet supplies energy via baroclinic conversion (Fig.7 middle), which is transferred to the rear side of the COL. The energy dispersion occurs via ageostrophic fluxes oriented in a northeastward direction (Fig. 7 top) and evolves in a wave train propagation that alternates with divergence and convergence regions (negative and positive AFC), similar to Rossby wave pattern propagation (Müller et al. 2015). This process is a clear signature during the growth stage ($T = -48h$ and $T = -24h$) and is observed over the upstream ridge associated with the PV overturning region (Knippertz and Martin 2007; Ndarana and Waugh 2010; Ndarana et al. 2021; Barnes et al. 2021). During the whole life cycle, the fluxes act to transport energy from the rear to the front of the COL,

contributing to the decay of the rear EKE center and growth of the front EKE center, as discussed above. Such transfer of energy reaches a maximum strength between $T = -24h$ and $T = 0$. The vertical cross-sections show that the energy transfer occurs preferably at high levels where the ageostrophic winds have a major contribution. However, when the COLs are considered individually rather than as a composite, some cases can exhibit the largest values of AFC at mid-levels simultaneously with intensification of baroclinicity (not shown). This configuration has also been observed in midlatitude disturbances, such as in the mature stage of the Storms *Friedhelm* and *Klaus* in the North Atlantic Ocean (Rivière et al. 2015) where the ageostrophic fluxes are found to be larger at ~500 hPa.

The integrated and vertical distributions of the BRC term provide a comprehensive picture of the baroclinic process and its contribution to the development of COLs. This is given in Figs. 7 and 8 (middle). The BRC conversion from EAPE to EKE occurs whenever the thermally direct circulation is active. As discussed before, the upstream energy source associated with the midlatitude jet is the primary mechanism for intensifying COLs. The energy transfer via ageostrophic fluxes maximizes between T $= -48h$ and $T = -24h$ together with local baroclinic processes that take place just behind the COL because of the sinking cold air (see also supplementary material Fig. S1), characterized by the early BRC peak shown in Fig. 5. The western EKE source starts to decrease during the period of peak intensity, but then another energy source evolves further east, because of the ascending warm air at mid and upper tropospheric and lower stratospheric levels (responsible for the late BRC peak). The upward motion is likely reinforced due to latent heat release in the warm air, which generates EAPE and consequently intensifies the baroclinic conversion. This is a particular feature of the strongest COLs and hence longer lifetimes are observed compared to less intense

systems. The results of this paper are consistent with Gan and Dal Piva (2013) and Ndarana et al. (2021), though our composites show a greater contribution from baroclinic processes, particularly because of the enhanced ascent in the most intense COLs, a feature that has not been previously reported. The energetics of the strong COLs exhibit a similar pattern to those shown by Danielson et al. (2004) for extratropical cyclones, corroborating the existence of a vertical coupling between upper-level COLs and low-level cyclones, as discussed in Pinheiro et al. (2020b).

Regions of positive (negative) BRC seem to be spatially correlated with regions of negative (positive) AFC. The assumption of interdependence between the AFC and BRC terms has been checked by examining the spatial correlation between these terms. We find an average correlation coefficient of -0.6 between the AFC and BRC terms, suggesting that the energy produced (dissipated) via the BRC conversion is dispersed (accumulated) through the ageostrophic fluxes. The temporal correlation between the AFC and BRC terms (computed over a spherical cap of 15 degrees) is negative at all stages of the lifecycle, reaching its largest value (-0.86) near the time of maximum intensity of the COLs. The combined action of the two mechanisms discussed above constitutes to the downstream baroclinic development.

The spatial composite of BRT conversion (Fig. 7 bottom) indicates that most of the COL region is dominated by negative values, particularly upstream from the COL center in the growth phase. This means that the horizontal shear upstream from the COL contributes to the zonal flow that extracts kinetic energy from the COL. In contrast, a minor contribution associated with barotropic conversion (positive values) occurs on the eastern EKE center in the late stages, though this is much less important than both the AFC and BRC processes. It is important to say that, despite the poor efficiency in generating kinetic energy, the barotropic instability was found to be the dominant

mechanism for the development of synoptic disturbances in tropical and subtropical regions (Colton 1973; Rao and Bonatti 1987; Mishra et al. 2001; 2007; Pinto and Rocha 2011).

3.4 Regional analysis

In section 3.2, the evolution of the main terms of the EKE budget were investigated. Here, the energetics are analyzed in detail using sector averages as these may vary regionally. The focus is on the sectors situated in the vicinity of the continents, which have been chosen based on the main genesis areas, selected over a spherical region (radius=10^{o}) centered on the maxima of genesis for eight regions (Fig. 9): A (32^{o}S, 10^{o}E), B (29^{o}S, 39^{o}E), C (33^{o}S, 105^{o}E), D (34^{o}S, 142^{o}E), E (33^{o}S, 161^{o}E), F (34^{o}S, 166^{o}E), G (34.5^{o}S, 80^{o}W) and H (35^{o}S 57^{o}W). The selection is made using all identified COLs (number of tracks for each region is indicated in the caption of Fig. 10), thus this guarantees that the analysis represents the typical EKE budget in each region. Fig. 10 shows the composite temporal evolution of the main energy terms with their corresponding standard deviation obtained in each of the eight regions. As expected, the two terms of the EKE budget that most contribute to the intensification of the COLs in all regions are BRC and AFC, while decay is dominated by dispersive ageostrophic fluxes (negative contribution of the AFC term) with BRT conversion (negative contribution) playing an important role in dissipating only the COLs in regions A, G and H (for more detail see Table I). There are, however, substantial regional differences in the relative contribution of the BRC and AFC terms for the intensification phase. We see that COLs formed upstream of the main continents (regions A, C and G) are clearly dominated by ageostrophic fluxes, as indicated by the largest maxima in AFC, agreeing with the results of Gan and Dal Piva (2013; 2016) for region G. This is also the case for the COLs in region B, though the ageostrophic fluxes are much weaker than those

associated with the COLs situated over the windward side of continents. On the other hand, the COLs located in southeast Australia and western Pacific (regions D, E and F) are mostly driven by baroclinic processes. For the COLs originating in sector H, the AFC and BRC terms contribute more or less equal to their growth. Although each region is influenced differently by each mechanism, there is a large variation in the contribution of the dominant mechanisms, particularly relating to the AFC that presents the highest standard deviation among all terms of the EKE budget.

Previous studies have suggested that the cut-off phenomena is a result of distinct RWB scenarios (Thorncroft and Mcintyre 1993; Ndarana and Waugh 2010; Portmann et al. 2020). The detailed analysis of the energy budget in different genesis regions suggests that the COLs originating in regions A, B, C and G may be influenced by stationary Rossby waves induced by surface topography that generally break anticyclonically, advecting high PV anomalies equatorward. The anticyclonic barotropic shear facilitates the transfer of EKE from the upstream midlatitude jet to the downstream EKE center associated with the COL, as demonstrated in earlier studies as well as here. While the downstream development appears to be the most important mechanism to COL growth in the aforementioned regions, the COLs that occur in southeast Australia, New Zealand and the western Pacific (regions D, E and F) are much less influenced by the ageostrophic fluxes. It is not clear what the reason for the differences are, but we hypothesize that the primary mechanisms for the evolution of a COL may be related to the circulation structure and the type of the RWB. Peters and Waugh (2003) showed that most of the RWB events in austral latitudes present an anticyclonic behavior with deformed PV contours tilting westward, while cyclonically RWB events (i.e., when PV contours tilt eastward and roll up cyclonically) are more common in the Australian region. This is likely caused by the presence of a split jet structure in the Australian

region, which becomes more apparent during the austral winter (Peters and Waugh 2003; Ndarana and Waugh 2011), though there is a large interannual variability (Elsholz et al. 2001). However, observational studies are too limited to cover the wide range of scenarios, and such assumptions need further study.

4 Discussion and conclusions

The results of this study provide insights into the main development mechanisms in austral COLs by analyzing the relative contributions of the components of the EKE budget for the most intense COLs across the whole hemisphere and also within eight regions of interest. The AFC together with the BRC conversion are found to be the primary mechanisms for the COL development. Results provide evidence of an interdependent association between the downstream energy fluxes and BRC conversion as these processes act by cancelling each other. Over the regions where the BRC term is positive (negative), the AFC tends to be negative (positive) as the ageostrophic fluxes act to export (import) the kinetic energy created (destroyed) by BRC conversion downstream (from upstream). The AFC is crucial for the formation and intensification of the COLs, while the BRC conversion is important throughout their lifecycle, representing the main mechanism to maintain the system.

The development of COLs agrees well with that described by Orlanski and Sheldon (1993) in which cyclone waves grow initially due to the energy dispersed by upstream systems and later because of the baroclinic conversion. The EKE life cycle of COLs is not particularly unique, rather it is variation in the development of typical midlatitude disturbances. There is, however, an important difference between the results described above and the conceptual model of Orlanski and Sheldon (1993), as the decay stage of the strong COLs is marked by an overturning and a partial interruption of the energy wave train propagation likely as a consequence of the Rossby wave breaking. This can

be seen, for example, in the ageostrophic fluxes orientated south-westward in the decay stage, thus redistributing the EKE within the system. This characteristic seems to be what differentiates the energetics of the COLs from a regular trough.

The initial preconditioning mechanism takes place upstream of the upper-level trough that will originate the COL, where a source region along the midlatitude jet supplies kinetic energy via baroclinic conversion, which is exported to the rear side of the incipient COL. The ageostrophic fluxes converge into the domain that give rise to net ageostrophic flux convergence and EKE growth during the development phase and net ageostrophic flux divergence and EKE decay during the decay phase. The processes described above occur simultaneously in each sector of the COL, but the magnitude of the AFC varies throughout the lifecycle, thus the EKE tendency will depend on the dominant relation between convergence and divergence of ageostrophic fluxes.

While the ageostrophic fluxes contribute to the EKE growth only during the growth stage, the BRC conversion is the only term that remains positive over the entire life cycle, representing the main EKE source for the COLs. Results have shown that the BRC conversion is important for both formation and maintenance of COLs, presenting two distinct peaks during their life cycle. The first one occurs in the development phase and is mainly associated with descent of cold air along the western edge of the COL cold core. The second peak occurs in the decay phase and is due to the ascent of warm air on the eastern side of the COLs, which occurs within the stratospheric warm core and extends down to a warm region further east (shown in the supplementary material, Fig. S1). The EKE production related to the BRC conversion maximizes in regions of strong temperature gradients around the vortex and is a robust feature of the strongest COLs, indicating that baroclinic processes are consistently more frequent in the main baroclinic zones. These findings complement the recent study by Pinheiro et al.

(2020b), and extend their observations on the structural features to a more dynamical view of the energetics of the strong COLs.

While the composite features support evidence of downstream development in COLs, the results do not seem to be robust enough to represent the wide variety of possible development scenarios. The regional analysis reveals substantial differences in the relative contributions of the main energetics terms in eight sectors in the SH. For example, the groups of COLs originating upstream of the continents are characterized by a large contribution of ageostrophic fluxes, while those systems located in the Australian region have weak ageostrophic geopotential fluxes and are mainly driven by baroclinic conversion. This shows that the upstream influence in the Australian COLs is quite weak compared to other regions, and suggests that such differences may occur in response to the type of Rossby wave breaking, as discussed before.

Another question that naturally arises is what makes the COLs so strong? Sensitivity analysis based on the system intensity (not shown) reveals that the mechanisms leading to increasing energy in the strongest systems (e.g., AFC and BRC conversion) are large enough to compensate the large effect of the damping mechanisms such as the BRT conversion and friction. In addition, diabatic mechanisms that occur during the development of the COLs may contribute to their further intensification.

One of the issues in exploring the EKE budget with reanalysis data is the relatively large residual observed by the composites, particularly from the mature to decay stages of the COLs (see Figs 3 and 4). One factor that may contribute to the residual is the unknown contribution from the friction, which is difficult to assess because this is “not computed directly, but is obtained as the residual arising out of any imbalance among the other terms” (Frank 1970). It is also possible that other mechanisms that are not addressed directly in this paper may affect the EKE budget, such as the fluxes related to

the volume displacement (terms 10-12 of Equation 1) and the reanalysis errors in the diabatic processes. Several studies have suggested that the primary effect of latent heat release is to produce a cyclonic PV anomaly in the lower troposphere and an anticyclonic PV anomaly in the upper troposphere (Davis and Emanuel 1991; Stoelinga 1996). This relationship is in agreement with earlier investigations (Sakamoto and Takahashi 2005; Garreaud and Fuenzalida 2007; Portmann et al. 2018) which have consistently shown that the latent heat release weakens upper-level COLs. The effect of the mid-tropospheric heating source in COLs is to modify the thermal structure and to result in upper-level divergent flow, then leading to an anticyclonic PV anomaly in the upper troposphere and the system weakening/dissipating. However, if the latent heat source is located in the warm sector of the COLs (for example, on their eastern border), it creates EAPE and we would expect an increase in the upward motion, and consequently an intensification of the COL through the BRC conversion. Similarly, the cloud-top radiative cooling in cold descent regions is expected to increase the EKE (Cavallo and Hakim 2010), resulting in a positive baroclinic conversion rate. As moisture-related processes can modify the vertical structure of potential vorticity, thereby influencing the development of disturbances, errors in diabatic heating in reanalysis could indirectly introduce errors in the EKE budget.

The accuracy of an estimate of the heating profiles depends on the consistency in which the large-scale circulation and thermodynamic fields are represented in the reanalyses. Particularly, the heating estimates based on the large-scale circulation depends on the estimates of divergence and vertical velocity, which are more susceptible to errors associated with low-resolution data. In the case of diabatic heating based on microphysical processes from reanalysis products, the estimates are more influenced by parameterization of moist processes in the assimilation schemes, which are more

important in the tropics (Katsumata et al. 2011; Hagos et al. 2012; Ling and Zhang 2013). The issues described above could be dealt with more easily by using numerical models, though there are uncertainties in the estimates of diabatic heating profiles by the models. The vertical distribution of diabatic heating is not fairly represented primarily by the models based on convective parameterization, however, using high-resolution numerical models in which cloud microphysics are treated explicitly may be able to simulate moist diabatic processes more realistically. Alternatively, there are methods that can be employed to estimate the diabatic contribution, for example, by using the thermodynamic equation (Caron et al. 2006) or a PV framework (Stoelinga 1996). Therefore, further work is clearly needed to determine how diabatic forcing modifies the dynamics of COLs and their energetics.

It is worth mentioning that the residual may also be due to computational errors associated with the numerical methods such as the analysis frequency and other unknown mechanisms. In this regard, a part of the uncertainties in the energetic calculations can be overcome by using higher temporal resolution data, such as the ERA5 reanalysis (Hersbach and Dee 2016), to compute a shorter time difference for the LHS of Equation 1. Another problem in most reanalysis systems is the analysis increment added to the background state's fields, thus the analysis increment caused by the changes to the first guess field can result in inconsistencies in the energetic analysis. Simmons et al. (2014) have shown, for example, a temperature analysis increment of up to 0.4 K in the ERA-Interim reanalysis.

Although compositing is a useful technique to investigate the typical aspects of COLs (Pinheiro et al. 2020b), a better understand of the case-to-case variability in terms of the ageostrophic fluxes and conversions is needed to yield new insights into the different nature of COLs. To deal with the wide variety of development scenarios, an

investigation of individual cases with respect to their evolution could be considered in future work, perhaps by undertaking a cluster analysis to identify the cases through similarities, or even using the vorticity budget which was found to be less case dependent due to its non-linearity (Azad and Sorteberg 2014).

This study has addressed some potential questions associated with the COL development, but a key question still remains unresolved: why some COLs lead to surface cyclogenesis and others remain confined at upper levels. The study of Rivière et al. (2015) found that vertical ageostrophic fluxes are important for the redistribution of energy downwards, and the further intensification of extratropical winter storms in the Northern Hemisphere. These vertical fluxes have been checked in this study and their contribution was found to be very small compared to the other terms considered in the discussion above. Further research could investigate the possible mechanisms underlying the deepening of COLs through the vertical modal decomposition in terms of kinetic energy and available potential energy, similarly to Silva Dias et al. (1985). Furthermore, it would therefore be of interest to investigate the possible interaction between COLs and wavetrains of troughs and ridges (wave packets) as the development of upstream systems in geographically remote regions may impact on the local energetics of a COL, as discussed in previous studies (Orlanski and Sheldon 1995; Chang 2000; Wirth et al. 2018).

The issues discussed here are points that need future research in order to obtain a more realistic view of which mechanisms and environmental factors influence the development of COLs. Despite the issues pointed out above, this study leads to substantial improvements in the knowledge of COLs, contributing to new perspectives on the more relevant influence of the downstream baroclinic development on COLs. This demonstrates that the analysis of various components of the EKE budget combined

with compositing are useful tools for investigating the evolution of synoptic-scale systems from reanalysis or model datasets.

Acknowledgements

This study was partly supported by CNPq (Conselho Nacional de Desenvolvimento Científico e Tecnológico) and CAPES (Coordenação de Aperfeiçoamento de Pessoal de Nível Superior). ERA-Interim data are freely available from the ECMWF public datasets web interface (http://apps.ecmwf.int/datasets). The TRACK algorithm is available on the University of Reading's Git repository (GitLab) at https://gitlab.act.reading.ac.uk/pub.

References

Azad, R. and Sorteberg, A. (2014) The vorticity budgets of North Atlantic winter extratropical cyclone life cycles in MERRA reanalysis. Part I: Development phase. *Journal of the Atmospheric Sciences,* **71**(9), 3109-3128.

Barnes, M. A., Ndarana, T., and Landman, W. A. (2021). Cut-off lows in the southern Hemisphere and their extension to the surface. *Climate Dynamics*, 1-24.

Bengtsson, L., Hodges, K.I., Esch, M., Keenlyside, N., Kornblueh, L., Luo, J. J. and Yamagata, T. (2007) How may tropical cyclones change in a warmer climate? *Tellus, Series A: Dynamic Meteorology and Oceanography*, **59**(4), 539-561.

Bozkurt, D., Rondanelli, L., Garreaud, R. and Arriagada, A. (2016) Impact of warmer eastern tropical Pacific SST on the March 2015 Atacama floods. *Monthly Weather Review* **144**(11), 4441-4460.

Buzzi, G. D., Tibaldi, S. and Tosi, E. (1987) A unified theory of orographic influences upon cyclogenesis. *Meteorology and Atmospheric Physics*, **36**, 91-107.

744 Carlson, T. N. (1991) *Mid-latitude weather systems*. [S.l]: Harper Collins Academic,
745 507 p.

746 Caron, J-F., Zwack, P. and Pagé, C. (2006) DIONYSOS: A diagnostic tool for
747 numerically-simulated weather systems. *Atmos.-Ocean, submitted. Technical related*
748 *document*, available in http://www. dionysos. uqam. ca/doc/Dionysos. pdf, 2006.

749 Catto, J.L, Shaffrey, L.C. and Hodges, K.I. (2010) Can climate models capture the
750 structure of extratropical cyclones? *Journal of Climate* **23**(7), 1621-1635.

751 Cavallo, S.M. and Hakim, G.J. (2010) Composite structure of tropopause polar
752 cyclones. *Monthly weather review* **138**(10), 3840-3857.

753 Chang, E.K.M. (1993) Downstream development of baroclinic waves as inferred from
754 regression analysis. *Journal of the Atmospheric Sciences*, **50**(13), 2038-2053.

755 Chang E.K.M. (2000) Wave packets and life cycles of troughs in the upper troposphere:
756 examples from the Southern hemisphere summer season of 1984/85. *Monthly Weather*
757 *Review*, **128**, 25-50.

758 Chang, E.K. and Orlanski, I. (1993) On the dynamics of a storm track. *Journal of*
759 *Atmospheric Sciences* **50**(7), 999-1015.

760 Chang E.K.M. and Orlanski, I. (1994) On energy flux and group velocity of waves in
761 baroclinic flows. *Journal of the Atmospheric Sciences*, **51**(24), 3823-3828.

762 Charney, J.G. (1947) The dynamics of long waves in a baroclinic westerly current.
763 *Journal of Meteorology*, **4**(5), 136-162.

764 Colton, D.E. (1973) Barotropic scale interactions in the tropical upper troposphere
765 during the northern summer. *Journal of the Atmospheric Sciences*, **30**, 1287-1302.

766 Dal Piva, E.D., Gan, M.A. and Rao, V.B. (2010) Energetics of winter troughs entering
767 South America. *Monthly Weather Review*, **138**(4), 1084-1103.

768 Dal Piva, E. and Gan, M.A. (2011) The role of latent and sensible heat fluxes in an
769 explosive cyclogenesis over the South American East coast. *Journal of the*
770 *Meteorological Society of Japan*, **86**(6), 637-663.

771 Danielson, R.E., Gyakum, J.R. and Straub, D.N. (2004) Examples of downstream
772 baroclinic development among 41 cold-season eastern North Pacific cyclones.
773 *Atmosphere-Ocean*, **42**(4), 235-250.

774 Danielson, R.E., Gyakum, J.R. and Straub, D.N. (2006) A case study of downstream
775 baroclinic development over the North Pacific Ocean. Part II: diagnoses of eddy energy
776 and wave activity. *Monthly Weather Review*, **134**(5), 1549-1567.

777 Davis, C.A. and Emanuel, K.A. (1991) Potential vorticity diagnostics of cyclogenesis.
778 *Monthly Weather Review* **119**(8), 1929-1953.

779 Davis, C.A, Stoeling, M.T. and Kuo, Y. (1993) The integrated effect of condensation in
780 numerical simulations of extratropical cyclogenesis. *Monthly Weather*
781 *Review*, **121**, 2309-2330.

782 Decker, S.G. and Martin, J.E. (2005) A local energetics analysis of the life cycle
783 differences between consecutive, explosively deepening, continental cyclones. *Monthly*
784 *Weather Review*, **133**(1), 295-316.

785 Eady, E.T. (1949) Long waves and cyclone waves. *Tellus*, **1**(3), 33-52.

786 Frank, N.L. (1970) On the energetics of cold lows. In: Symposium on Tropical
787 Meteorology. Proceedings… *American Meteorological Society* EIV1-EIV6.

788 Fuenzalida, H.A., Sánchez, R. and Garreaud, R.D. (2005) A climatology of cutoff lows
789 in the Southern Hemisphere. *Journal of Geophysical Research* 110:D18101.

790 Gan, M.A. and Rao, V.B. (1994) The influence of the Andes Cordillera on transient
791 disturbances. *Monthly Weather Review*, **122**(6), 1141-1157.

Gan, M.A. and Dal Piva, E. (2013) Energetics of a Southeastern Pacific cut-off low. *Atmospheric Science Letters* **14**(4), 272-280.

Gan, M.A. and Dal Piva, E.D. (2016) Energetics of southeastern Pacific cut-off lows. *Climate Dynamics*, **46**(11-12), 3453-3462.

Garreaud, R.D. and Fuenzalida, H.A. (2007) The influence of the Andes on cutoff lows: a modeling study. *Monthly Weather Review* **135**(4), 1596-1613.

Guo, Y. and Chang, E.K. (2008) Impacts of assimilation of satellite and rawinsonde observations on Southern Hemisphere baroclinic wave activity in the NCEP–NCAR reanalysis. *Journal of climate*, **21**(13), 3290-3309.

Hagos, S., Zhang, C., Tao, W. K., Lang, S., Takayabu, Y. N., Shige, S. et al. (2010) Estimates of tropical diabatic heating profiles: Commonalities and uncertainties. *Journal of Climate*, **23**(3), 542-558.

Hayashi, Y. (1970) A theory of large-scale equatorial waves generated by condensation heat and accelerating. *Journal of the Meteorological Society of Japan. Ser. II*, **48**(2), 140-160.

Hayes, J.L., Williams, R.T. and Rennick, M.A. (1987) Lee cyclogenesis. Part I. analytic studies. *Journal of the Atmospheric Sciences*, **44**(2), 432-442.

Hodges, K.I. (1994) A general Method for tracking analysis and its application to meteorological data. *American Meteorological Society*, **122**, 2573-2585.

Hodges, K.I. (1995) Feature tracking on the unit sphere. Mon. Wea. Rev.,**123**, 3458-3465.

Hodges, K.I. (1999) Adaptive constraints for feature tracking. Mon. Wea.Rev.,**127**, 1362-1373

Hoskins, B.J., Mcintyre, M.E. and Robertson, A.W. (1985) On the use and significance of isentropic potential vorticity maps. *Quarterly Journal of the Royal Meteorological Society* **111**(470), 877-946.

Katsumata, M., Ciesielski, P.E., and Johnson, R.H. (2011) Evaluation of budget analyses during MISMO. *Journal of Applied Meteorology and Climatology* **50**(1), 241-254.

Knippertz, P. and Martin, J.E. (2007) The role of dynamic and diabatic processes in the generation of cut-off lows over Northwest Africa. Meteorology and Atmospheric Physics **96**(1), 3-19.

Kousky, V.E. and Gan, M.A. (1981) Upper tropospheric cyclonic vortices in the subtropical South Atlantic. *Tellus* **33**(6), 538-551.

Kuo, H.L. (1949) Dynamic instability of two-dimensional non-divergent flow in a baroclinic atmosphere. *Journal of Meteorology* **6**(2), 105-122.

Kuo, Y., Low-Nam, S. and Reed, R.J. (1991) Effects of surface energy fluxes during the early development and rapid intensification stages of seven explosive cyclones in the Western Atlantic. *Monthly Weather Review*, **119**, 457-476.

Lamb, V.R. (1973) The response of the tropical atmosphere to middle latitude forcing. *PhD thesis, University of California, Los Angeles*, **155**, 151p.

Ling, J. and Zhang, C. (2013) Diabatic heating profiles in recent global reanalyses. *Journal of Climate* **26**(10), 3307-3325.

Llasat, M.C., Martín, F. and Barrera, A. (2007) From the concept of "Kaltlufttropfen" (cold air pool) to the cut-off low. The case of September 1971 in Spain as an example of their role in heavy rainfalls. Meteorology and Atmospheric physics 96(1-2), 43-60.

Lorenz, E.N. (1955) Available potential energy and the maintenance of the general circulation. *Tellus*, **7**(2), 157-167.

Magaña, V. and Yanai, M. (1995) Mixed Rossby-gravity waves triggered by lateral forcing. *Journal of the atmospheric sciences*, **52**(9), 1473-1486.

Mak, M.K. (1969) Laterally driven stochastic motions in the tropics. *Journal of the Atmospheric Sciences*, **26**(1), 41-64.

Martínez-Alvarado, O. and Plant, R.S. (2014) Parametrized diabatic processes in numerical simulations of an extratropical cyclone. *Quarterly Journal of the Royal Meteorological Society*, **140**(682), 1742-1755.

McInnes, K.L., and Hubbert, G.D. (2001) The impact of eastern Australian cut-off lows on coastal sea levels. *Meteorological Applications: A journal of forecasting, practical applications, training techniques and modelling*, **8**(2), 229-243.

Mcintyre, M.E and Palmer, T.N. (1983) Breaking planetary waves in the stratosphere. *Nature*, **305**, 593-600.

Michaelides, S.C. (1987) Limited area energetics of genoa cyclogenesis. *Monthly Weather Review*, **115**(1), 13-26.

Mikyfunatsu, B., Gan, M.A. and Caetano, E. (2004) A case study of orographic cyclogenesis over South America. *Revista Atmosfera* **17**(2), 91-113.

Mishra, S.K., Rao, V.B. and Gan, M.A. (2001) Structure and evolution of the large-scale flow and an embedded upper-tropospheric cyclonic vortex over northeast Brazil. *Monthly Weather Review*, **129**(7), 1673-1688.

Mishra, S.K., Rao, V.B. and Franchito, S.H. (2007) Genesis of the northeast brazil upper-tropospheric cyclonic vortex: A primitive equation barotropic instability study. *Journal of the Atmospheric Sciences,* **64**(4), 1379-1392.

Muench, H.S. (1965) On the dynamics of the wintertime stratosphere circulation. *Journal of the Atmospheric Sciences*, **22**(4), 349-360.

Muller, A., Reason, C.J.C. and Fauchereau, N. (2008) Extreme rainfall in the Namib Desert during late summer 2006 and influences of regional ocean variability. *International Journal of Climatology: A Journal of the Royal Meteorological Society,* **28**(8), 1061-1070.

Müller, G.V., Gan, M.A., Dal Piva, E., and Silveira, V.P. (2015) Energetics of wave propagation leading to cold event in tropical latitudes of South America. *Climate Dynamics* **45**(1-2), 1-20.

Ndarana, T. and Waugh, D.W. (2010) The link between cut-off lows and Rossby wave breaking in the Southern Hemisphere. *Quarterly Journal of the Royal Meteorological Society* **136**(649), 869-885.

Ndarana, T. and Waugh, D.W. (2011) A climatology of Rossby wave breaking on the Southern Hemisphere tropopause. *Journal of the Atmospheric Sciences* **68**(4), 798-811.

Ndarana, T., Rammopo, T.S., Chikoore, H., Barnes, M.A. and Bopape, M.J. (2020) A quasi-geostrophic diagnosis of the zonal flow associated with cut-off lows over South Africa and surrounding oceans. *Climate Dynamics* **55**(9), 2631-2644.

Ndarana, T., Rammopo, T.S., Bopape, M.J., Reason, C.J. and Chikoore, H. (2021) Downstream development during South African cut-off low pressure systems. *Atmospheric Research* **249**, 105315.

Nieto, R., Sprenger, M., Wernli, H., Trigo, R.M. and Gimeno, L. (2008) Identification and climatology of cut-off low near the tropopause. *Annals of the New York Academy of Sciences* **1146**(1), 256-290.

Nogués-Paegle, J. and Mo, K.C. (1997) Alternating wet and dry conditions over South America during summer. *Monthly Weather Review*, **125**, 279-291.

Oort, A.H. and Peixoto, J.P. (1983) Global angular momentum and energy balance requirements from observations. *Advances in Geophysics*, **25**, 355-490.

Orlanski, I. and Katzfey, J. (1991) The life cycle of a cyclone wave in the Southern Hemisphere: eddy energy budget. *Journal of the Atmospheric Sciences*, **48**, 1972-1998.

Orlanski, I. and Chang, E.K. (1993) Ageostrophic geopotential fluxes in downstream and upstream development of baroclinic waves. *Journal of Atmospheric Sciences* **50**(2), 212-225.

Orlanski, I. and Sheldon, J.P. (1993) Case of downstream baroclinic development over Western North America. *Monthly Weather Review*, **121**, 2929- 2950.

Orlanski, I. and Sheldon, J.P. (1995) Stages in the energetics of baroclinic systems. *Tellus*, **47a**, 605-628.

Papritz, L. and Schemm, S. (2013) Development of an idealised downstream cyclone: Eulerian and Lagrangian perspective on the kinetic energy. *Tellus A: Dynamic Meteorology and Oceanography* **65**(1), 19539.

Pedlosky, J. (1987) Geophysical Fluid Dynamics. *2.ed. Berlin: Springer-Verlag*.

Peters, D. and Waugh, D. W. (2003) Rossby wave breaking in the Southern Hemisphere wintertime upper troposphere. *Monthly weather review* **131**(11), 2623-2634.

Pinheiro, H.R., Hodges, K.I., Gan, M.A. and Ferreira, N.J. (2017) A new perspective of the climatological features of upper-level cut-off lows in the Southern Hemisphere. *Climate Dynamics* **48**(1-2), 541-559.

907 Pinheiro, H.R., Hodges, K.I. and Gan, M.A. (2019) Sensitivity of identifying Cut-off
908 Lows in the Southern Hemisphere using multiple criteria: implications for numbers,
909 seasonality and intensity. *Climate Dynamics* **53**(11), 6699-6713.
910 Pinheiro, H.R., Hodges, K.I. and Gan, M.A. (2020a) An intercomparison of Cut-off
911 Lows in the subtropical Southern Hemisphere using recent reanalyses: ERA-Interim,
912 NCEP-CFSR, MERRA-2, JRA-55, and JRA-25. *Climate Dynamics* **54**, 777-792.
913 Pinheiro, H., Gan, M. and Hodges, K. (2021) Structure and evolution of intense austral
914 cut-off lows. *Quarterly Journal of the Royal Meteorological Society* **147**(734), 1-20.
915 Pinto, J.R.D. and da Rocha, R.P. (2011) The energy cycle and structural evolution of
916 cyclones over southeastern South America in three case studies. *Journal of Geophysical*
917 *Research: Atmospheres,* (116.D14).
918 Poli, P., Hersbach, H., Dee, D. P., Berrisford, P., Simmons, A. J., Vitart, F., ... and
919 Fisher, M. (2016) ERA-20C: An atmospheric reanalysis of the twentieth
920 century. *Journal of Climate* **29**(11), 4083-4097.
921 Pook, M.J., Mcintosh, P.C. and Meyers, G.A. (2006) The synoptic decomposition of
922 cool-season rainfall in the southeastern Australian cropping region. *Journal of Applied*
923 *Meteorology and Climatology*, **45**(8), 1156-1170.
924 Portmann, R., Crezee, B., Quinting, J. and Wernli, H. (2018) The complex life cycles of
925 two long-lived potential vorticity cut-offs over Europe. *Quarterly Journal of the Royal*
926 *Meteorological Society* **144**(712), 701-719.
927 Portmann, R., Sprenger, M. and Wernli, H. (2020) The three-dimensional life cycle of
928 potential vorticity cutoffs: A global ERA-interim climatology (1979–2017). *Weather*
929 *and Climate Dynamics Discussions* 1-52.

Privé, N. C. and Errico, R. M. (2013) The role of model and initial condition error in numerical weather forecasting investigated with an observing system simulation experiment. *Tellus A: Dynamic Meteorology and Oceanography*, **65**(1), 21740.

Rao, V.B. and Bonatti, J.P. (1987) On the origin of upper tropospheric cyclonic vortices in the South Atlantic Ocean and adjoining Brazil during the summer. *Meteorology and Atmospheric Physics*, **37**(1), 11-16.

Reboita, M.S., Nieto, R., Gimeno, L., Rocha, R.P., Ambrizzi, T., Garreaud, R. and Kruger, L.F. (2010) Climatological features of cutoff low systems in the Southern Hemisphere. *Journal of Geophysical Research: Atmospheres* **115**, D17104.

Risbey, J.S., Pook, M.J., Mcintosh, P.C., Ummenhofer, C.C. and Meyers, G. (2009) Characteristics and variability of synoptic features associated with cool season rainfall in southeastern Australia. *International Journal of Climatology*, **29**(11), 1595-1613.

Rivière, G., Arbogast, P. and Joly, A. (2015) Eddy kinetic energy redistribution within windstorms Klaus and Friedhelm. *Quarterly Journal of the Royal Meteorological Society*, **141**(688), 925-938.

Rossby, C.G. (1945) On the propagation of frequencies and energy in certain types of atmospheric and oceanic waves. *Journal of Meteorology*, **2**(4), 187-204.

Sakamoto. K. and Takahashi M. (2005) Cut off and weakening processes of an upper cold low. *Journal of the Meteorological Society of Japan*, **83**, 817-834.

Schemm, S., Wernli, H. and Papritz, L. (2013) Warm conveyor belts in idealized moist baroclinic wave simulations. *Journal of the Atmospheric Sciences* **70**(2), 627-652.

Silva Dias, P.L., Schubert, W.H. and Demari, M. (1983) Large-scale response of the tropical atmosphere to transient convection. *Journal of the Atmospheric Sciences*, **40**(11), 2689-2707.

Silva Dias, P.L. and Bonatti, J.P. (1985) A preliminary study of the observed vertical mode structure of the summer circulation over tropical South America. *Tellus A*, **37**(2), 185-195.

Simmons, A.J. and Hoskins, B.J. (1979) The downstream and upstream development of unstable baroclinic waves. *Journal of Atmospheric Sciences* **36**(7), 1239-1254.

Simmons, A.J., Poli, P., Dee, D.P., Berrisford, P., Hersbach, H., Kobayashi, S., and Peubey, C. (2014) Estimating low-frequency variability and trends in atmospheric temperature using ERA-Interim. *Quarterly Journal of the Royal Meteorological Society*, ***140***(679), 329-353.

Singleton, A.T. and Reason, C.J.C. (2007) A Numerical model study of an intense cutoff low pressure system over South Africa. *Monthly Weather Review* **135**(3), 1128-1150.

Stoelinga, M.T. (1996) A potential vorticity-based study of the role of diabatic heating and friction in a numerically simulated baroclinic cyclone. *Monthly Weather Review* **124**(5), 849-874.

Thorncroft, C.D., Hoskins, B.J. and McIntyre, M. E. (1993) Two paradigms of baroclinic-wave life-cycle behaviour. *Quarterly Journal of the Royal Meteorological Society* **119**(509), 17-55.

Willmott, A.J. (1985) A note on the steepening of long Rossby waves. Deep Sea Research Part A. *Oceanographic Research Papers*, **32**(5), 613-617.

Wirth, V., Riemer, M., Chang, E. K. and Martius, O. (2018) Rossby wave packets on the midlatitude waveguide - A review. *Monthly Weather Review* **146**(7), 1965-2001.

Yanai, M. and Maruyama, T. (1966) Stratospheric wave disturbances propagating over the equatorial Pacific. *Journal of the Meteorological Society of Japan*. Ser. II, **44**(5), 291-294.

Yeh, T.C. (1949) On energy dispersion in the atmosphere. *Journal of Meteorology*, **6**, 1-16.

Figure/Captions

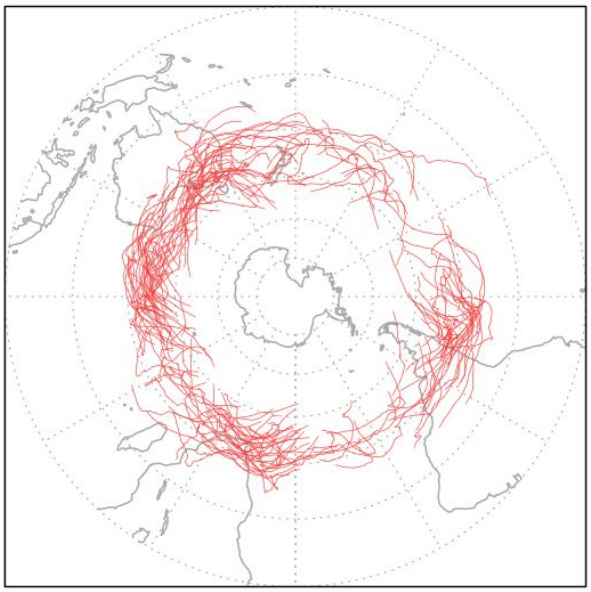

Figure 1 Trajectories of the 200 most intense Cut-off Lows in the Southern Hemisphere identified in both ξ_{300} and Z'_{300}. Red lines indicate the trajectories obtained at each 6-hourly time step.

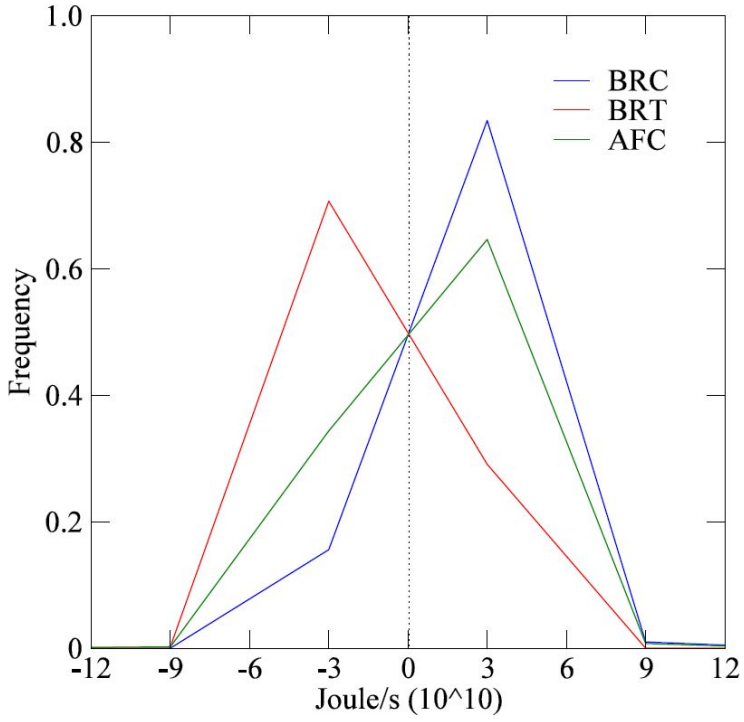

Figure 2 Frequency distribution of the SH COLs for the along-track mean components of the EKE budget: BRC (blue line), BRT (red line), AFC (green line). Fields are vertically averaged within a 15° spherical cap region centered on the COL location. Unit is Joule s^{-1}, scaled by 10^{10}.

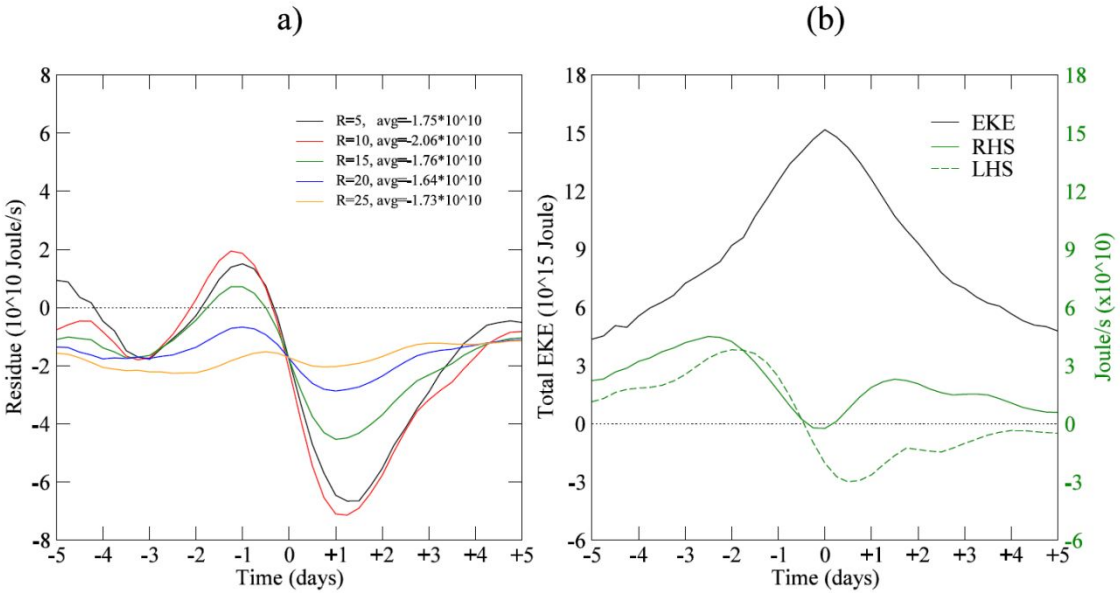

Figure 3 Temporal evolution of the strongest COLs for a) residual and b) total EKE and EKE tendencies. Composites of the 200 most intense SH COLs that match between the ξ_{300} and Z'_{300}, relative to the time of maximum intensity in ξ_{300}. Residual values are determined using different spherical cap regions (r=5°, 10°, 15°, 20° and 25°) centered on the COL location. The inset indicates the average of residue within the corresponding area. The total EKE and their tendencies are determined within a 15° spherical cap region centered on the COL center. Tendencies are computed using RHS

(solid line) and LHS (dashed line). Unit is Joule s^{-1} for residuals and tendencies (scaled by 10^{10}) and Joule for the total EKE (scaled by 10^{15}). All these quantities are vertically averaged from surface to 100 hPa.

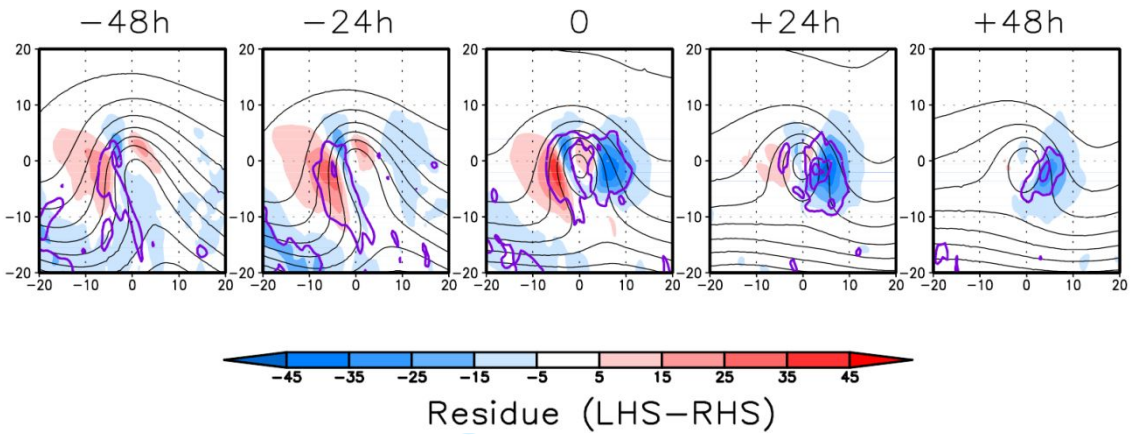

Figure 4 Temporal evolution of the residue (shaded) and its standard deviation (purple line) for the strongest COLs. Composites of the 200 most intense SH COLs that match between the ξ_{300} and Z'_{300}, relative to the time of maximum intensity in ξ_{300}. Residue is computed by the difference between LHS and RHS of Equation 1. Unit is 10^{10} Joule s^{-1}. Z_{300} height in denotes in black lines for 100 gpm contours.

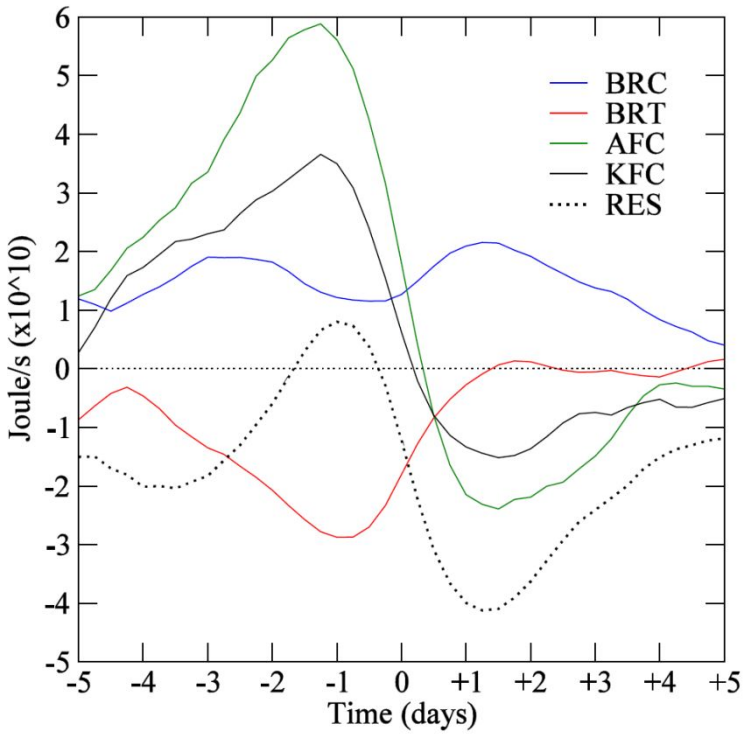

Figure 5 Temporal evolution of the main EKE terms in the strongest COLs. The terms are BRC (blue line), BRT (red line), AFC (green line), KFC (black line) and RES (dotted line). Fields are vertically averaged within a 15° spherical cap region centered on the COL location. Unit is Joule s^{-1}, scaled by 10^{10}.

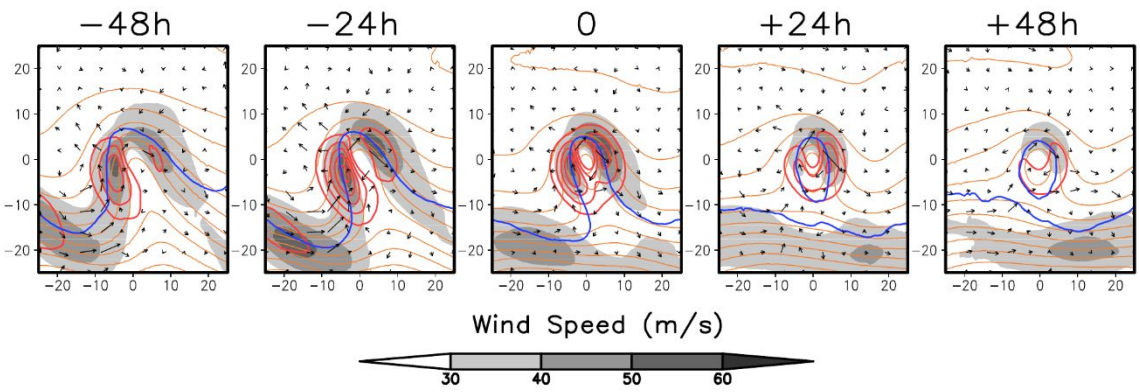

Figure 6 Temporal evolutions of the 200 strongest Cut-off Lows in the SH that match between the ξ_{300} and Z'_{300}, relative to the time and space of maximum intensity in ξ_{300}. Fields are the total vertically integrated EKE (red line) for 500 $\times$ 10^{10} Joule contours, wind speed in m.s^{-1} (shaded), Z_{300} height for 100 gpm contours (orange line), -2.0 PVU on the 330 K surface, and integrated ageostrophic fluxes (vectors). The distance from the center of the composite to the edge is 25°.

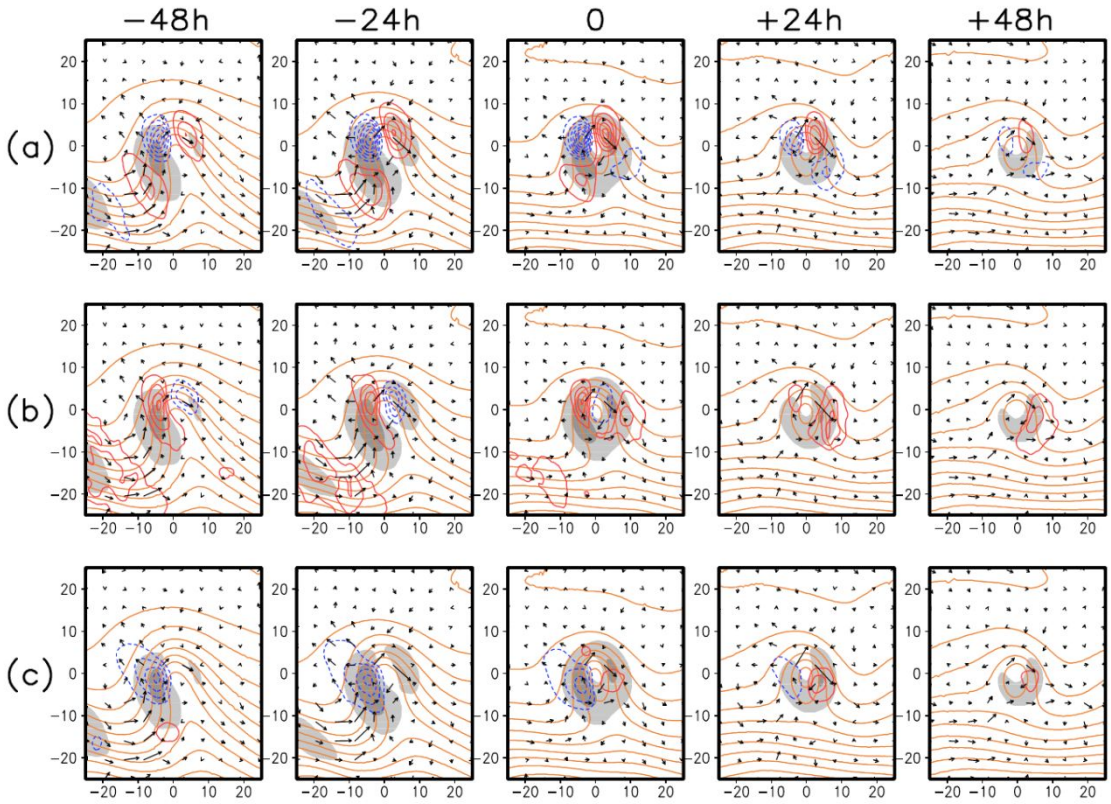

Figure 7 Same as Fig. 5 but for the total EKE together with main EKE terms: AFC (upper), BRC (middle) and BRT (bottom). Fields are the total vertically integrated EKE (shaded) for 1000-1500 x 10^{10} Joule intervals, the Z_{300} height (orange line) for 100 gpm intervals, combined with vertically average fields of AFC for 20 x 10^{10} Joule s^{-1} intervals, BRC and BRT for 5 x 10^{10} Joule s^{-1} intervals, where positive (negative) values are indicated in red (blue).

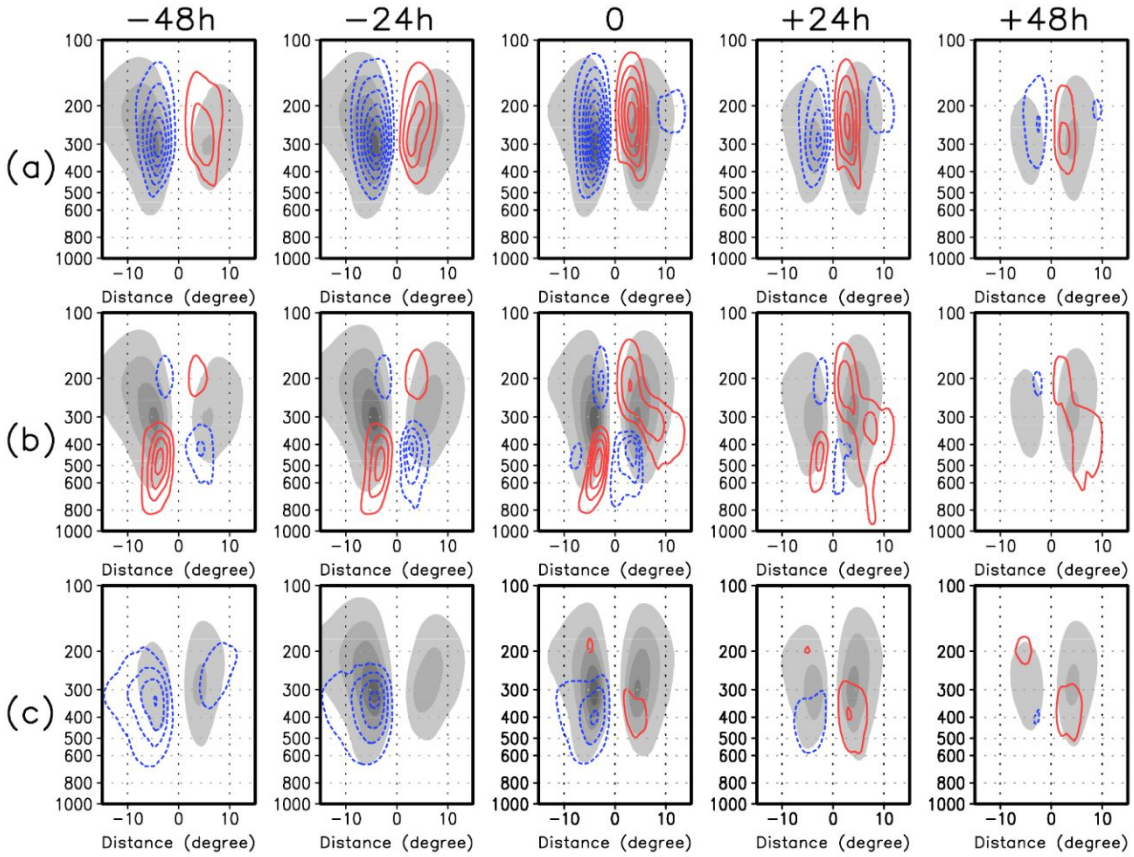

Figure 8 Same as Fig. 7 but for the vertical cross sections of the total EKE combined with (a) AFC, (b) BRC, and (c) BRT. Intervals are 300 x 10^{10} Joule for the total EKE (shaded), 1.5 x 10^{10} Joule s^{-1} for the AFC term (contour), and 0.3 x 10^{10} Joule s^{-1} for the BRC and BRT terms (contour). Positive (negative) values are indicated in red (blue).

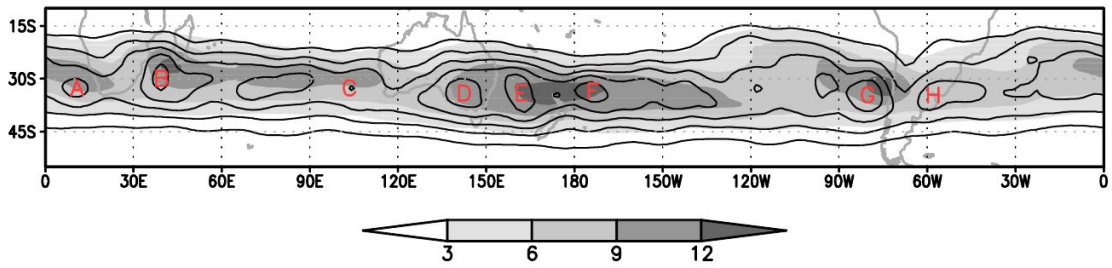

Figure 9 Track density (shaded) and genesis density (contour) of all identified Cut-off Lows. Maximum genesis is denoted by regions A(32°S 10°E), B(29°S 39°E), C(33°S 105°E), D(34°S 142°E), E(33°S 161°E), F(34°S 166°E), G(34.5°S 80°W) and H(35°S 57°W). Unit is number per season per unit area, the unit area is equivalent to a 5° spherical cap (≅10^6 km^2).

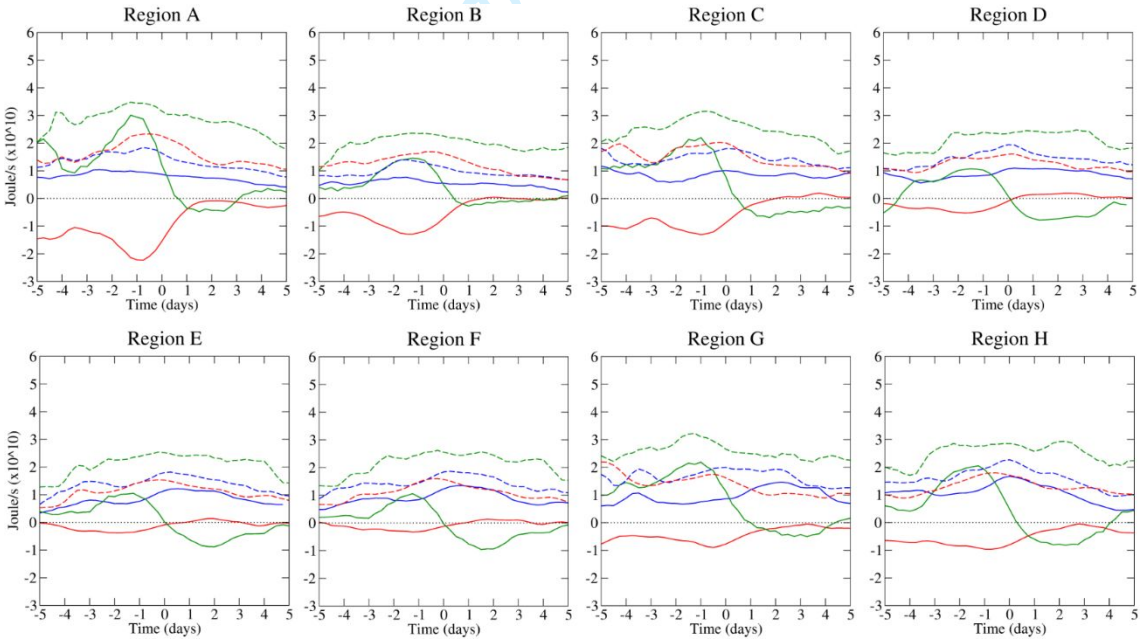

Figure 10 Same as Fig. 5 but for the eight regions defined in Fig. 9. The terms BRC (blue), BRT (red) and AFC (green) are given in solid line with their corresponding standard deviation in dashed line. The number of tracks for each region are: 741 (A), 950 (B), 746 (C), 1042 (D), 1048 (E), 1047 (F), 804 (G) and 611 (G).

Table I Accumulated contribution of the main terms of EKE budget for eight regions defined in Fig. 9. The terms are baroclinic (BRC) and barotropic (BRT) conversions and ageostrophic flux convergence (AFC). The growth phase (from day -5 to day 0) and decay phase (from day 0 to day +5) are determined with regard to the time of maximum intensity. Unit is Joule s^{-1}, scaled by 10^{10}.

	Growth stage			*Decay stage*		
	BRC	BRT	AFC	BRC	BRT	AFC
A	**18.2**	**-31.2**	**38.5**	**13.1**	**-6.0**	**-0.9**
B	12.4	-17.6	17.1	9.1	-1.2	-1.8
C	**16.9**	**-20.7**	**30.0**	**17.1**	**-0.9**	**-8.1**
D	15.5	-7.4	11.9	19.3	2.1	-10.9
E	**13.8**	**-5.1**	**12.2**	**18.8**	**0.1**	**-9.9**
F	16.0	-4.1	9.8	19.7	0.8	-10.6
G	**15.5**	**-12.7**	**32.0**	**22.9**	**-4.8**	**-2.9**
H	23.1	-15.8	24.4	19.3	-5.8	-7.4

Contributions of downstream baroclinic development to strong Southern Hemisphere Cut-off Lows

Henri Rossi Pinheiro*, Manoel Alonso Gan, Kevin Ivan Hodges, Sergio Henrique Soares Ferreira, and Kelen Martins Andrade

This study provides a new perspective of the main development mechanisms in Cut-of Lows (COLs) by analyzing the relative contributions of the components of eddy kinetic energy budget for the 200 strongest austral COLs. Composite COLs show that the ageostrophic flux convergence (AFC) together with the baroclinic conversion are the most important contributor to the energy growth, characterizing the downstream baroclinic development. The typical development of the COLs involves an interdependent association between the AFC and the baroclinic terms as these processes act by cancelling each other.

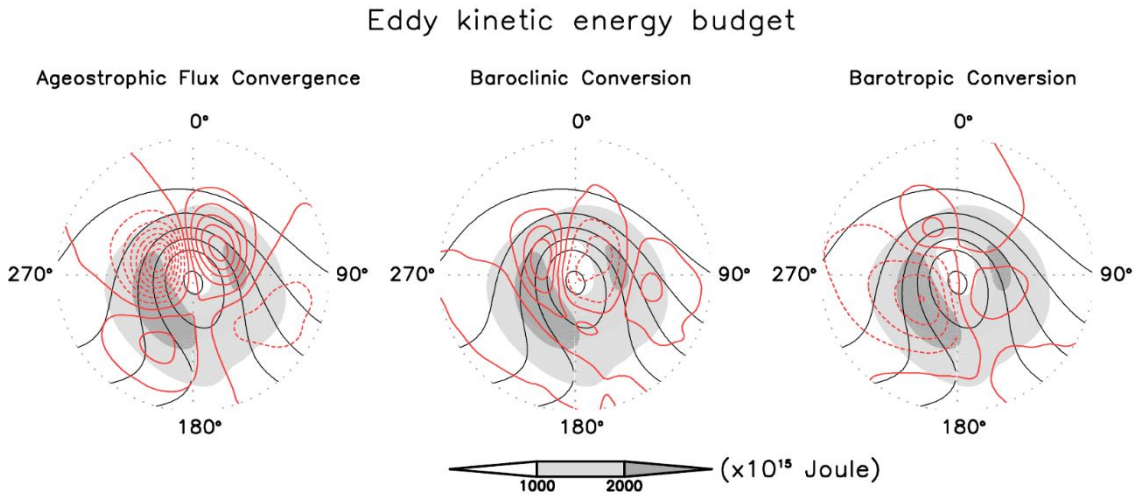

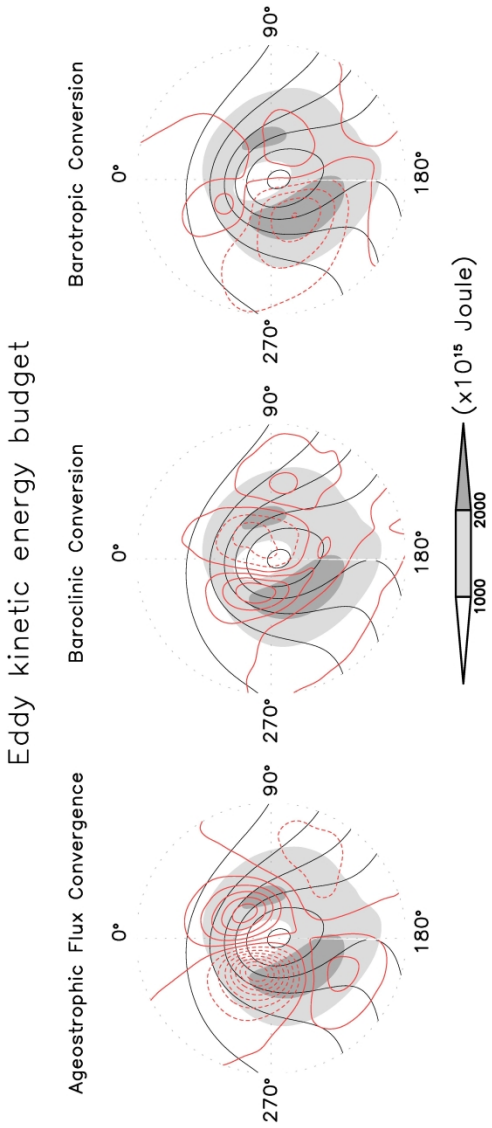

184x256mm (600 x 600 DPI)

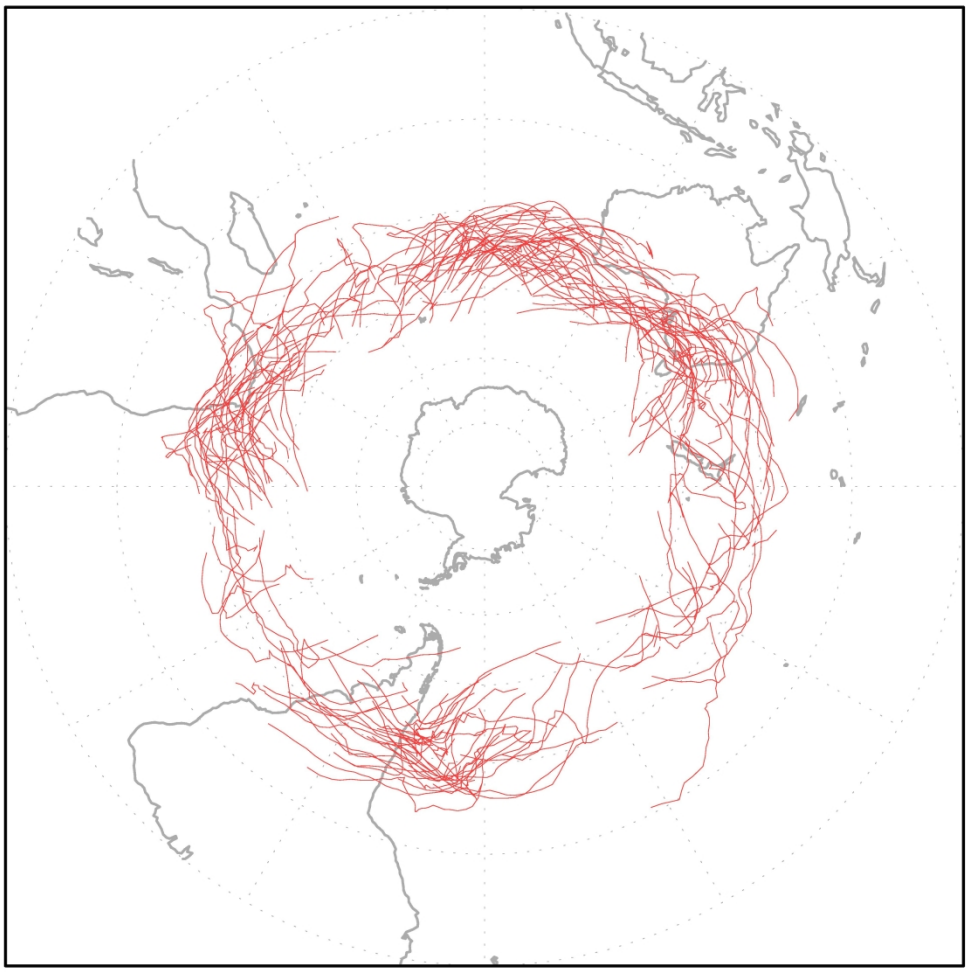

Trajectories of the 200 most intense Cut-off Lows in the Southern Hemisphere identified in both ξ_{300} and Z'_{300}. Red lines indicate the trajectories obtained at each 6-hourly time step.

169x188mm (600 x 600 DPI)

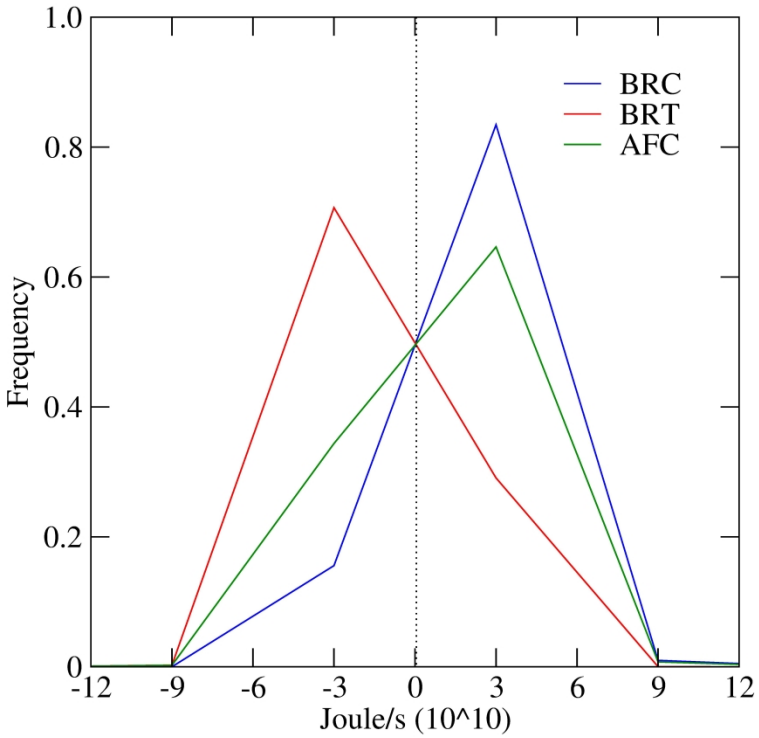

Frequency distribution of the SH COLs for the along-track mean components of the EKE budget: BRC (blue line), BRT (red line), AFC (green line). Fields are vertically averaged within a 15^{o} spherical cap region centred on the COL location. Unit is Joule s^{-1}, scaled by 10^{10}.

215x279mm (600 x 600 DPI)

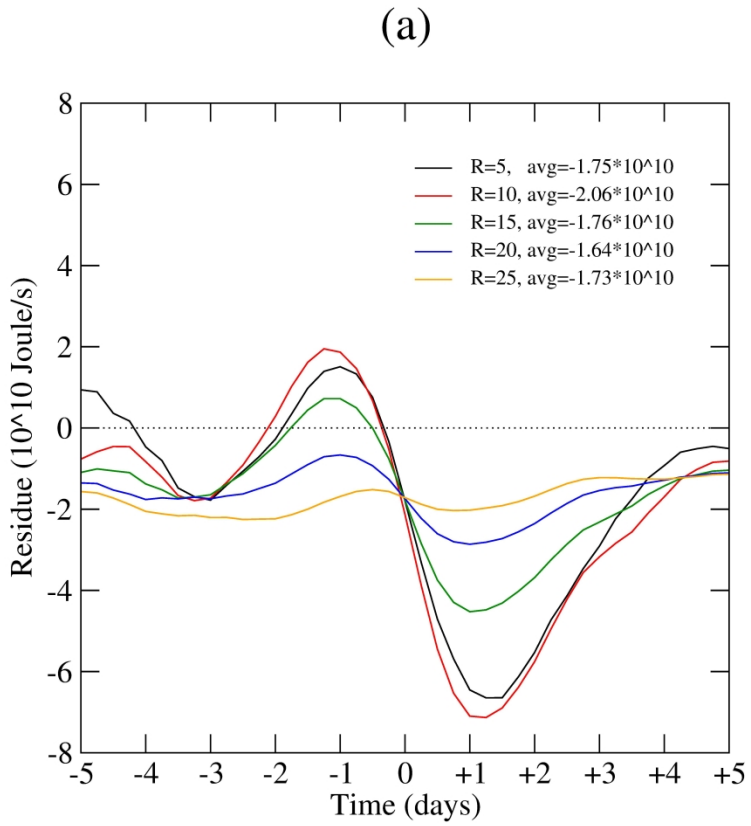

Temporal evolution of the strongest COLs for (a) residual and (b) total EKE and EKE tendencies. Composites of the 200 most intense SH COLs that match between the ξ_{300} and Z_{300}', relative to the time of maximum intensity in ξ_{300}. Residual values are determined using different spherical cap regions (r=5°, 10°, 15°, 20° and 25°) centred on the COL location. The inset indicates the average of residue within the corresponding area. The total EKE and their tendencies are determined within a 15° spherical cap region centred on the COL centre. Tendencies are computed using RHS (solid line) and LHS (dashed line). Unit is Joule s^{-1} for residuals and tendencies (scaled by 10^{10}) and Joule for the total EKE (scaled by 10^{15}). All these quantities are vertically averaged from surface to 100 hPa.

215x279mm (600 x 600 DPI)

(b)

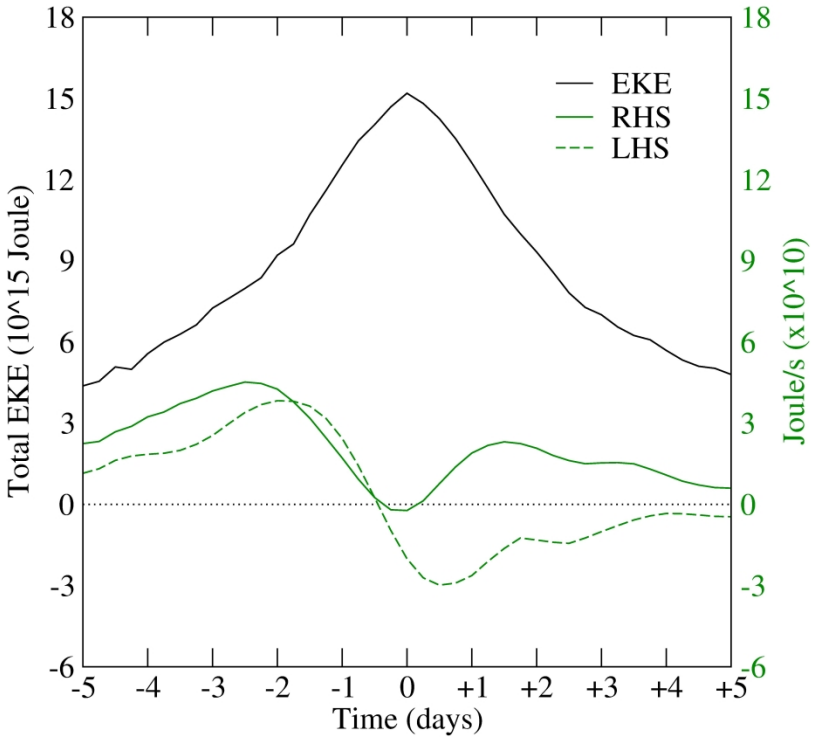

215x279mm (600 x 600 DPI)

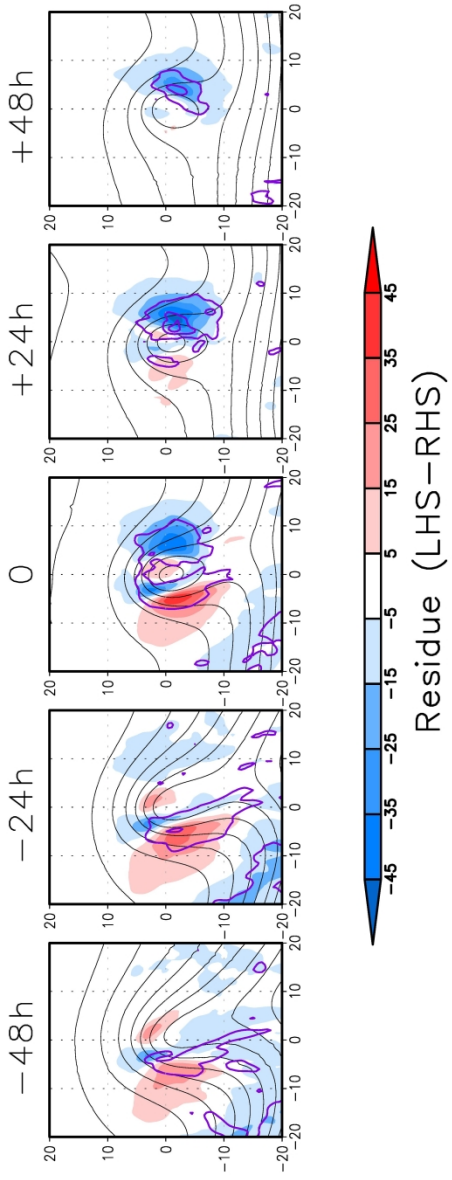

Temporal evolution of the residue (shaded) and its standard deviation (purple line) for the strongest COLs. Composites of the 200 most intense SH COLs that match between the ξ_{300} and Z_{300}', relative to the time of maximum intensity in ξ_{300}. Residue is computed by the difference between LHS and RHS of Equation 1. Unit is 10^{10} Joule s^{-1}. Z_{300} height is denoted in black lines for 100 gpm contour.

162x239mm (600 x 600 DPI)

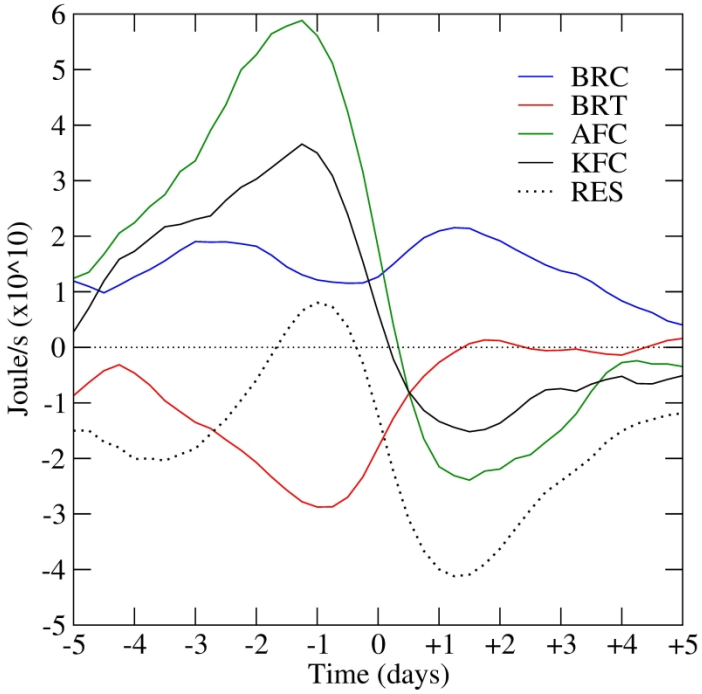

Temporal evolution of the main EKE terms in the strongest COLs. The terms are BRC (blue line), BRT (red line), AFC (green line), KFC (black line) and RES (dotted line). Fields are vertically averaged within a 15^{o} spherical cap region centred on the COL location. Unit is Joule s^{-1}, scaled by 10^{10}.

209x297mm (600 x 600 DPI)

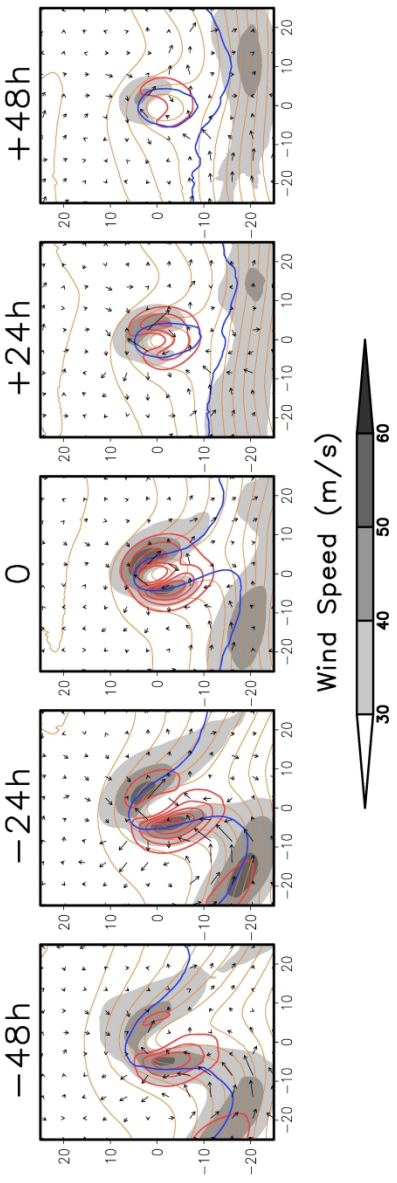

Temporal evolutions of the 200 strongest Cut-off Lows in the SH that match between the ξ_{300} and Z_{300}', relative to the time and space of maximum intensity in ξ_{300}. Fields are the total vertically integrated EKE (red line) for 500 × 10^{10} Joule contours, wind speed in m s^{-1} (shaded), Z_{300} height for 100 gpm contours (orange line), -2.0 PVU on the 330 K surface, and integrated ageostrophic fluxes (vectors). The distance from the centre of the composite to the edge is 25°.

161x237mm (600 x 600 DPI)

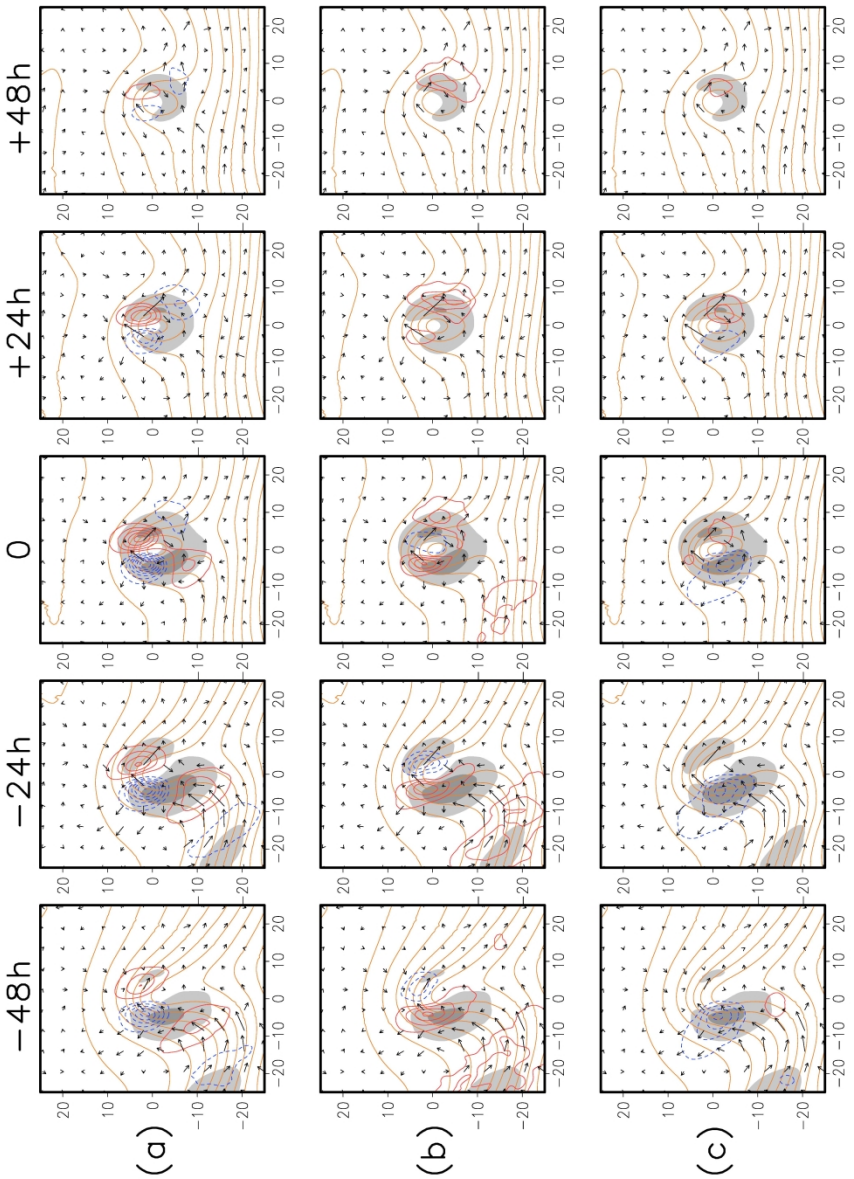

Same as Fig. 5 but for the total EKE together with main EKE terms: AFC (upper), BRC (middle) and BRT (bottom). Fields are the total vertically integrated EKE (shaded) for 1000-1500 x 10^{10} Joule intervals, the Z_{300} height (orange line) for 100 gpm intervals, combined with vertically average fields of AFC for 20 x 10^{10} Joule s^{-1} intervals, BRC and BRT for 5 x 10^{10} Joule s^{-1} intervals, where positive (negative) values are indicated in red (blue).

179x247mm (600 x 600 DPI)

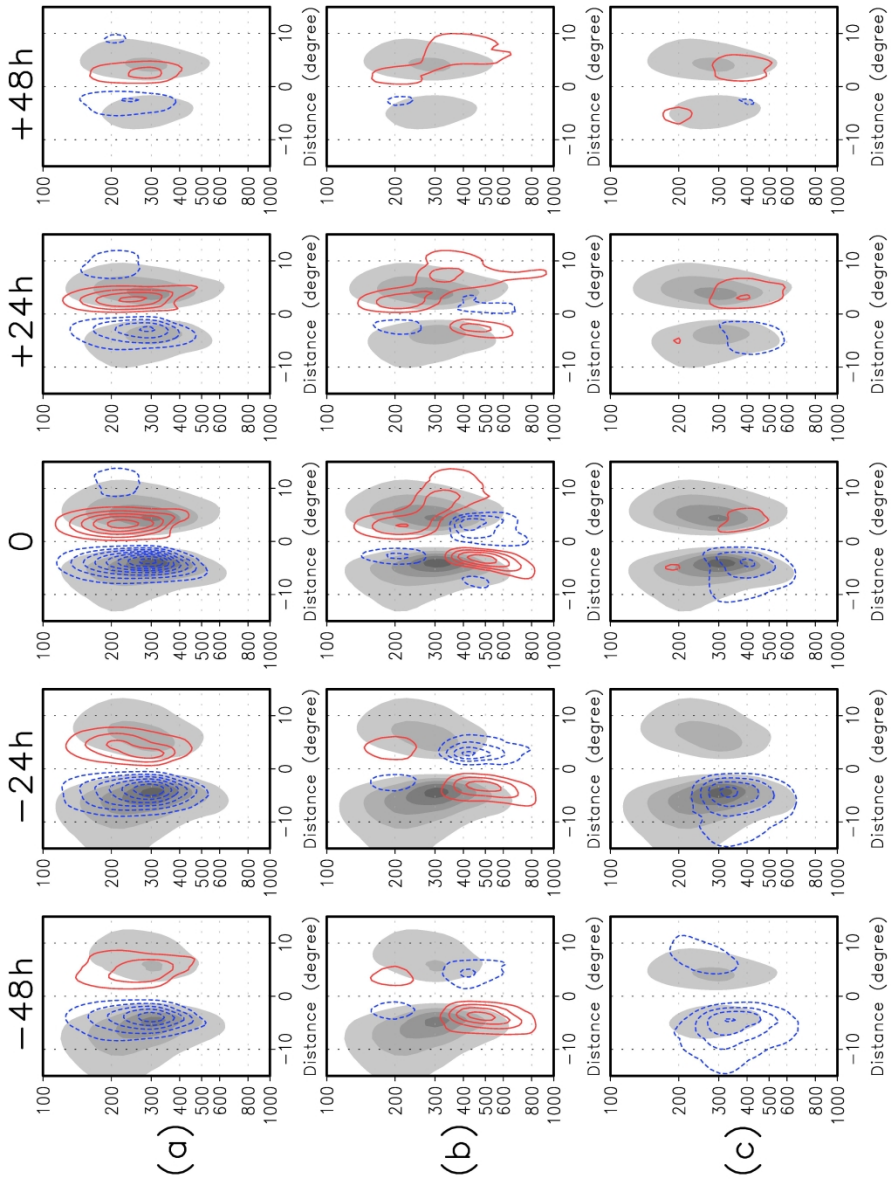

Same as Fig. 7 but for the vertical cross sections of the total EKE combined with (a) AFC, (b) BRC, and (c) BRT. Intervals are 300 x 10^{10} Joule for the total EKE (shaded), 1.5 x 10^{10} Joule s^{-1} for the AFC term (contour), and 0.3 x 10^{10} Joule s^{-1} for the BRC and BRT terms (contour). Positive (negative) values are indicated in red (blue).

186x244mm (600 x 600 DPI)

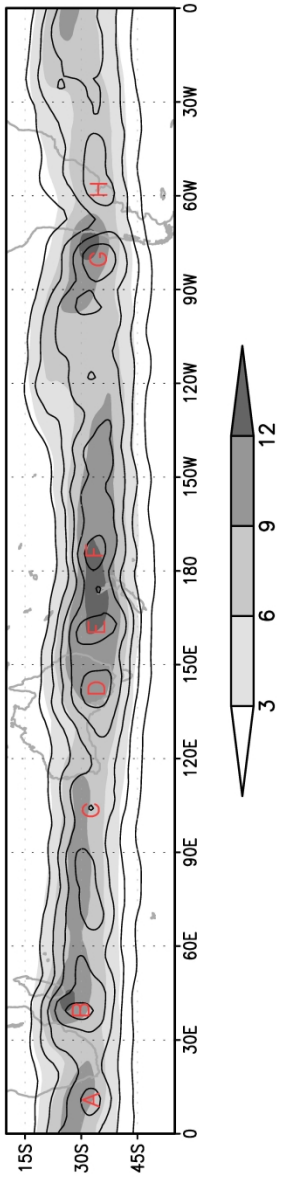

Track density (shaded) and genesis density (contour) of all identified Cut-off Lows. Maximum genesis is denoted by regions A(32^{o}S 10^{o}E), B(29^{o}S 39^{o}E), C(33^{o}S 105^{o}E), D(34^{o}S 142^{o}E), E(33^{o}S 161^{o}E), F(34^{o}S 166^{o}E), G(34.5^{o}S 80^{o}W) and H(35^{o}S 57^{o}W). Unit is number per season per unit area, the unit area is equivalent to a 5^{o} spherical cap ($\cong 10^{6}$ km^{2}).

95x247mm (600 x 600 DPI)

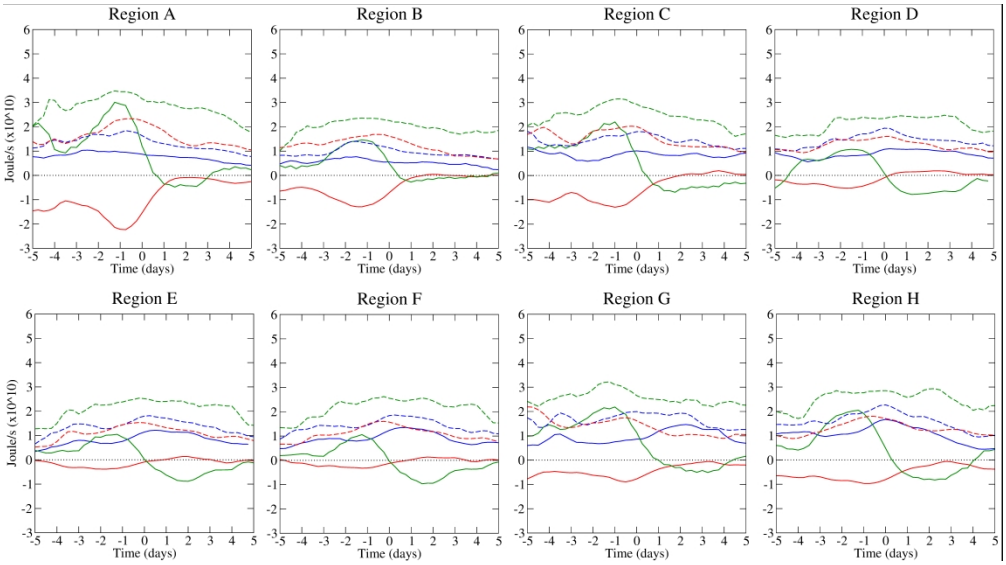

Same as Fig. 5 but for the eight regions defined in Fig. 9. The terms BRC (blue), BRT (red) and AFC (green) are given in solid line with their corresponding standard deviation in dashed line. The number of tracks for each region are: 741 (A), 950 (B), 746 (C), 1042 (D), 1048 (E), 1047 (F), 804 (G) and 611 (G).

345x192mm (600 x 600 DPI)

	Growth stage			*Decay stage*		
	BRC	BRT	AFC	BRC	BRT	AFC
A	**18.2**	**-31.2**	**38.5**	**13.1**	**-6.0**	**-0.9**
B	12.4	-17.6	17.1	9.1	-1.2	-1.8
C	**16.9**	**-20.7**	**30.0**	**17.1**	**-0.9**	**-8.1**
D	15.5	-7.4	11.9	19.3	2.1	-10.9
E	**13.8**	**-5.1**	**12.2**	**18.8**	**0.1**	**-9.9**
F	16.0	-4.1	9.8	19.7	0.8	-10.6
G	**15.5**	**-12.7**	**32.0**	**22.9**	**-4.8**	**-2.9**
H	23.1	-15.8	24.4	19.3	-5.8	-7.4

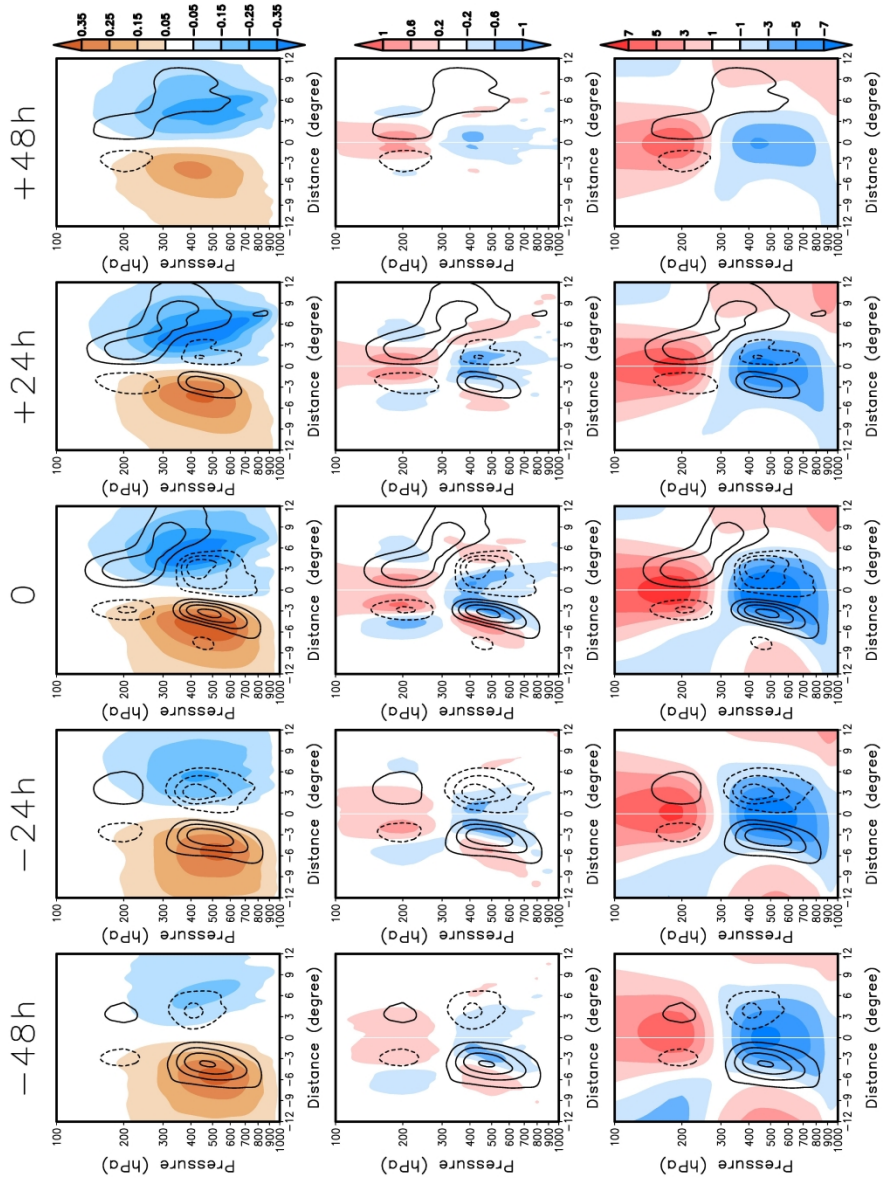

Lifecycle composite of the 200 most intense Cut-off Lows for the west-east vertical cross section. Fields are: (top) vertical velocity (shaded) in Pa s^{-1}; (middle) thermal frontal parameter (shaded) in 10^{-10} K $(100\ km)^{-2}$; and (bottom) temperature anomaly in K. All fields are combined BRC term in 0.3 x 10^{15} Joule day^{-1} contour intervals. Composites are centred on time and space relative to the ξ_{300} minimum

187x248mm (600 x 600 DPI)